

Estimating bedload from suspended load and water discharge in sand bed rivers

Thomas Ashley¹, Brandon McElroy¹, Daniel Buscombe², Matt Kaplinski², and Paul Grams³

¹University of Wyoming

²Northern Arizona University

³US Geological Survey

November 23, 2022

Abstract

Estimates of fluvial sediment discharge from in situ instruments are an important component of large-scale sediment budgets that track long-term geomorphic change. Suspended sediment load can be reliably estimated using acoustic or physical sampling techniques; however, bedload is difficult to measure directly and can consequently be one of the largest sources of uncertainty in estimates of total load. We propose a physically-informed predictive empirical model for bedload sand flux as a function of variables that are measured using existing acoustic or physical sampling techniques. This model depends on the assumption that concentration and grain size in suspension are in equilibrium with reach-averaged boundary conditions. Bayesian inference is used to fit model parameters to data from eight sand-bed rivers and to simulate bedload flux over the available gage record at one site on the Colorado River in Grand Canyon National Park. We find that the cumulative bedload flux during the nine year period from 2008 to 2016 was 5% of the cumulative suspended sand load; however, instantaneous bedload flux ranged from as little as 1% of instantaneous suspended sand load to as much as 75% of instantaneous suspended sand load due to fluctuations in flow strength and sediment supply. Changes in bedload flux at a constant discharge are indicative of short-term sediment supply enrichment and depletion. Long-term average bedload flux cannot be expected to remain constant in the future as the river adjusts to changes in sediment runoff and the dam-regulated discharge regime.

Abstract

Estimates of fluvial sediment discharge from in situ instruments are an important component of large-scale sediment budgets that track long-term geomorphic change. Suspended sediment load can be reliably estimated using acoustic or physical sampling techniques; however, bedload is difficult to measure directly and can consequently be one of the largest sources of uncertainty in estimates of total load. We propose a physically-informed predictive empirical model for bedload sand flux as a function of variables that are measured using existing acoustic or physical sampling techniques. This model depends on the assumption that concentration and grain size in suspension are in equilibrium with reach-averaged boundary conditions. Bayesian inference is used to fit model parameters to data from eight sand-bed rivers and to simulate bedload flux over the available gage record at one site on the Colorado River in Grand Canyon National Park. We find that the cumulative bedload flux during the nine year period from 2008 to 2016 was 5% of the cumulative suspended sand load; however, instantaneous bedload flux ranged from as little as 1% of instantaneous suspended sand load to as much as 75% of instantaneous suspended sand load due to fluctuations in flow strength and sediment supply. Changes in bedload flux at a constant discharge are indicative of short-term sediment supply enrichment and depletion. Long-term average bedload flux cannot be expected to remain constant in the future as the river adjusts to changes in sediment runoff and the dam-regulated discharge regime.

1 Introduction

Estimates of fluvial sediment load provide an important tool for quantifying large-scale geomorphic change. In a wide range of environments, suspended sediment load can be accurately constrained using acoustic surrogates for sediment concentration [Topping *et al.*, 2004; Topping & Wright, 2016], enabling low-cost measurement of suspended load at high temporal resolutions over multi-year timescales [Dean *et al.*, 2016; Grams *et al.*, 2013, 2018]. However, acoustic estimates of flux depend on assumptions about the vertical concentration distribution that are reasonable if not strictly valid in the interior of the flow [Gray & Gartner, 2010] but that become increasingly dubious in the near-bed region. Bedload may vary significantly with respect to suspended sediment load due to changes in Rouse conditions [van Rijn, 1984].

Existing procedures for measuring bedload separately from suspended load in sand-bedded rivers [Gray *et al.*, 2010; Holmes, 2019] are incompatible with the goals and limitations of long-term monitoring. Direct physical sampling is costly and can be inaccurate in large rivers due to undersampling [Pitlick, 1988], and existing predictive bedload transport models that might be used in lieu of direct measurements (e.g. Wong & Parker [2006]) generally require, at minimum, an estimate of the skin friction component of bed shear stress, which in turn necessitates additional measurements or models each subject to their own logistical limitations and uncertainty. Sediment budgets therefore rely on simplified treatments of bedload flux that can introduce large persistent biases to estimates of total bed material load. For example, bedload is typically estimated either as a constant fraction of suspended load [Grams *et al.*, 2013], a power-law function of water discharge (i.e. a rating curve) [Ellison *et al.*, 2016], or ignored [Wright *et al.*, 2010]. This is problematic because bedload flux can be a substantial fraction of total load in suspension-dominated rivers, particularly at low flow conditions [Turowski *et al.*, 2010]; bedload flux can vary relative to suspended load due changes in suspension conditions, and it can vary with respect to a fixed water discharge due to changes in bed material composition and channel geometry [Topping *et al.*, 2000a,b].

The purpose of this paper is to provide a reliable means for estimating bedload flux in sand-bed rivers when suspended sediment information is available. The rationale behind our approach is that bedload and suspended load are mutually determined by the same causal boundary conditions at the reach-averaged scale. As a result, measured changes in concentration and grain size in suspension can be used to deduce changes in these boundary conditions

and estimate bedload flux. This concept was first proposed by *Rubin & Topping* [2001] and underlies an empirical model that expresses bedload flux per unit channel width as a function of unit water discharge, suspended sand concentration, and suspended sand diameter.

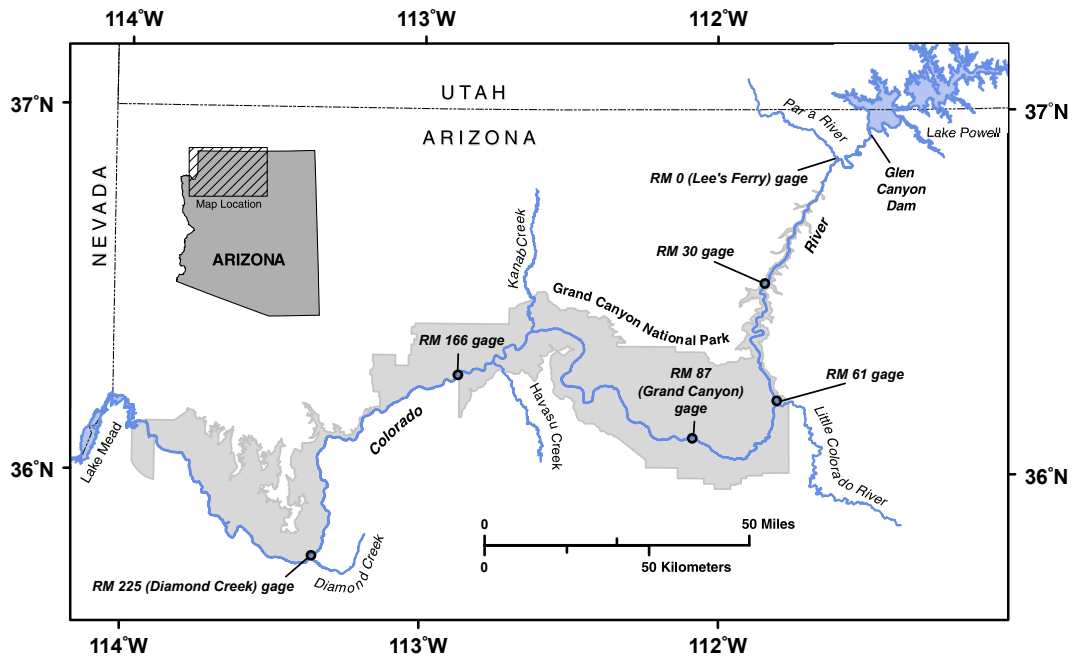
Our primary goal is to estimate bedload flux from gage data and propagate uncertainty through estimates of cumulative load. This is accomplished using Bayesian inference, which provides a convenient framework for quantifying uncertainty in sediment transport parameters using numerical Markov chain Monte-Carlo (MCMC) methods [*Schmelter et al.*, 2011; *Schmelter & Stevens*, 2012; *Schmelter et al.*, 2015]. Moreover, Bayesian techniques implemented in the MCMC framework enable rigorous propagation of uncertainty through individual estimates of sediment load and time-integrated mass balance calculations [*Schmelter et al.*, 2012].

Our model can be applied in any sand-bedded river and does not require site-specific calibration. However, our analysis reveals that predictions may be biased on a site-specific basis such that greater predictive accuracy is achieved when the model is fit using only data from one site. This is particularly important when computing sediment budgets because error associated with model bias accumulates over time [*Grams et al.*, 2013]. Unfortunately, site-specific data are not always available; in order to meet the varying needs of different applications, we present three modeling approaches that utilize historical data from seven rivers reported by *Toffaletti* [1968] to varying degrees. The first approach involves pooling all data to estimate model parameters and is acceptable for obtaining single estimates of bedload flux at sites where no direct observations are available. The second approach utilizes only data from the site of interest, and is suitable when extensive site-specific data are available. The third approach involves a hierarchical modeling framework [*Gelman et al.*, 1995; *Christensen et al.*, 2011] that optimizes use of limited site-specific data by using sites with many observations to inform prediction at sites with relatively few observations. Application of all three approaches is demonstrated at one sediment monitoring station on the Colorado river. The statistical procedure presented here ultimately provides a convenient method for tracking changes in bedload flux driven by flow strength and sediment supply limitation over timescales ranging from days to years.

2 Colorado River sediment monitoring

On the Colorado River in Grand Canyon National Park, flux-based sediment budgets inform flow regulation protocols aimed at minimizing the downstream impact of Glen Canyon Dam. The primary management objective is the reversal of long-term depletion of alluvial sand deposits, especially emergent deposits known as eddy sand bars, through the use of controlled floods [*Topping et al.*, 2010; *Wright & Kaplinski*, 2011; *Grams et al.*, 2015]. However, the range of available management solutions is limited; this objective must be accomplished without compromising other economic [*Ingram et al.*, 1991] and ecological [*Minckley*, 1991] objectives. Designing such a protocol requires a detailed understanding of the dynamics of flow and sediment transport through the canyon.

In the dam-regulated Colorado River, the upstream sediment supply is completely independent from water discharge. Undammed tributaries comprise the only resupply of alluvial material to the post-dam river, while the hydrograph is determined by clear water releases from Lake Powell [*Andrews*, 1991; *Topping et al.*, 2000a; *Rubin et al.*, 2002]. Sediment supply and flow fluctuations cause complex morphodynamic interactions as the channel adjusts to accommodate pulses of sediment under the imposed discharge regime. Confinement by bedrock and bouldery debris fans also limits the extent to which flow can modify local slope and hydraulic geometry. As a result, antecedent sedimentary and morphological conditions are as important as water discharge in regulating instantaneous sediment transport [*Rubin & Topping*, 2001]. This condition, known as “supply limitation,” is common in natural rivers, but is particularly pronounced on the Colorado River and other dammed rivers



136 **Figure 1.** Map of the Colorado River in Grand Canyon National Park, after *Grams et al.* [2013]). Data used
 137 in this study come from the reach adjacent to the Diamond Creek gage located at river mile 225.

116 due to artificial flow regulation and sediment starvation [*Dolan et al.*, 1974; *Schmidt & Graf*,
 117 1990].

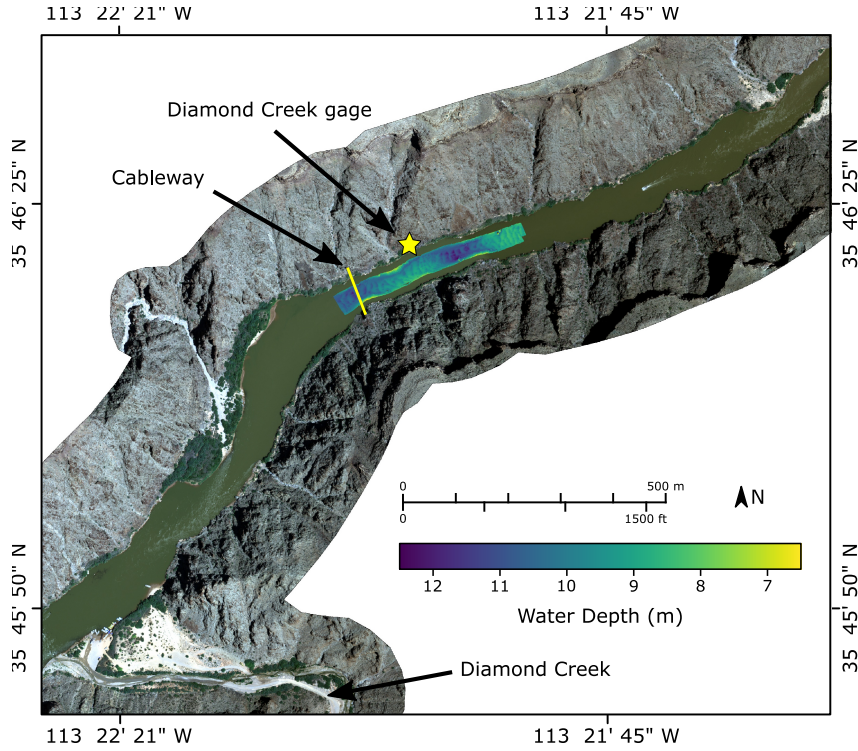
118 Modeling the dynamics of alluvial deposits in supply-limited systems requires substan-
 119 tial physical simplifications and empiricism (e.g. *Wright et al.* [2010]). Changes in stored
 120 sediment mass estimated from spatial gradients in sediment flux are a useful metric for eval-
 121 uating the effects of past flow regimes and for testing predictive models that can be used to
 122 determine best-practice scenarios for the future. The canyon is divided into five sediment
 123 budget reaches, each bounded by monitoring stations on the main stem and major tributaries
 124 that estimate total sand load every fifteen minutes (Figure 1). At the time of writing, these
 125 records comprise over a decade of almost uninterrupted suspended sediment data that can be
 126 used to quantify morphodynamic trends over a range of timescales: multi-year trends indi-
 127 cate regime-scale adjustment while short-term variability reflects the transient response to
 128 individual or seasonal perturbations in flow strength and sediment supply. Data are available
 129 online at https://www.gcmrc.gov/discharge_qw_sediment/.

130 Bedload flux is perhaps the largest source of uncertainty in estimates of total sediment
 131 load. At the time of writing, bedload is estimated at all monitoring sites on the Colorado
 132 River as a constant 5% of suspended load based on a single set of concurrent measurements
 133 of bedload and suspended load [*Rubin et al.*, 2001]. Presently, we aim test this assumption
 134 at one site (Figure 2), and reduce bias in estimates of total load by developing and applying a
 135 robust statistical methodology for estimating bedload flux from gage data.

140 **3 Methods and data**

141 **3.1 Modeling approach**

142 The goal of this paper is to predict total mass bedload flux, Q_b [MT^{-1}], from mea-
 143 surements of water discharge, suspended sand concentration, and suspended sand diame-
 144 ter. To this end, we adopt an empirical power-law equation for bedload flux per unit width



138 **Figure 2.** Aerial view of the Diamond Creek study site. One survey of water depth is plotted, illustrating
 139 the extent of the sonar mapping area.

145 q_b [$MT^{-1}L^{-1}$] given by:

$$q_b = Ae^{\beta_0} q_w^{\beta_1} C_s^{\beta_2} D_s^{\beta_3}. \quad (1)$$

146 Here, q_w [L^2/T] is the average volumetric water discharge per unit width equal to Q_w/W ,
 147 where Q_w [L^3/T] is the total volumetric water discharge and W [L] is the surface width of
 148 the channel. C_s [L/L] is the discharge-averaged suspended sand concentration, D_s [L]
 149 is median diameter of suspended sand and A is a dimensional coefficient expressed in terms of
 150 fixed reference values for each variable (denoted by the subscript 0) as $A = q_{b0}/q_{w0}^{\beta_1} C_{s0}^{\beta_2} D_{s0}^{\beta_3}$.
 151 Finally, β_0 is an intercept term that is equal to 0 if reference values are chosen so that $q_b =$
 152 q_{b0} when $q_w = q_{w0}$, $C_s = C_{s0}$, and $D_s = D_{s0}$.

153 Equation (1) is purely empirical; however, we consider the form of this expression in
 154 the context of existing theory to (1) facilitate qualitative interpretation of our results and (2)
 155 support the notion that in-sample fit will extend to out-of-sample predictive accuracy. For-
 156 ward models for equilibrium sediment transport [Einstein, 1950; McLean, 1992; Molinas
 157 & Wu, 2002; Wright & Parker, 2004] encompass the physical interactions that are relevant
 158 to this objective, and generally involve several computational steps that incorporate various
 159 physical and empirical expressions. As an example Wright & Parker [2004] proposed a com-
 160 putational procedure for estimating C_s , D_s , and the Shields' stress due to skin friction τ_{*s}
 161 (among other variables) from specified reach-average boundary conditions, which are q_w ,
 162 slope S [L/L], and bed material grain size D_b [L]. Bedload flux can be computed from τ_{*s}
 163 using an empirical bedload transport formula [e.g. Wong & Parker, 2006]. Additional rele-
 164 vant physical parameters that must be specified are often assumed to be constants. These are
 165 gravitational acceleration g [L/T^2], the kinematic viscosity of water ν [L^2/T], and the den-
 166 sities of sediment ρ_s [M/L^3] and water ρ_w [M/L^3]. In summary, this model approximates

167 three unknown physical equations of the following functional form:

$$q_b = f(q_w, S, D_b, \rho_s, \rho_w, g, \nu) \quad (2)$$

$$C_s = f(q_w, S, D_b, \rho_s, \rho_w, g, \nu) \quad (3)$$

$$D_s = f(q_w, S, D_b, \rho_s, \rho_w, g, \nu). \quad (4)$$

168 Each forward equation has eight variables (seven predictor variables and one response
169 variable) and three physical dimensions, and can therefore be reduced to five dimensionless
170 variables (four predictor variables and one response variable) according to the Buckingham
171 Pi theorem [Gibbins, 2011]. However, four of the eight physical variables are usually as-
172 summed to be constant so one of these dimensionless variables will always be a constant or
173 a linear combination of other variables. Assuming power-law forward equations between
174 dimensionless variables, we assert that any choice of dimensionless variables can be rear-
175 ranged to obtain the following dimensional equations:

$$q_b = \gamma_1 q_w^{\alpha_{11}} S^{\alpha_{12}} D_b^{\alpha_{13}} \quad (5)$$

$$C_s = \gamma_2 q_w^{\alpha_{21}} S^{\alpha_{22}} D_b^{\alpha_{23}} \quad (6)$$

$$D_s = \gamma_3 q_w^{\alpha_{31}} S^{\alpha_{32}} D_b^{\alpha_{33}} \quad (7)$$

176 where γ_1 , γ_2 , and γ_3 are fixed dimensional coefficients that can be expressed in terms of g , ν ,
177 ρ_s , and ρ_w . This system of equations can then be solved to obtain equation (1), noting that β_i
178 exponents are simply algebraic combinations of α_{ij} exponents.

179 Based on these arguments, we offer the following interpretation of equation (1), leav-
180 ing further discussion to Section 5.2. We assume changes in fluvial sediment transport con-
181 ditions are driven by changes in q_w , S , and D_b . By measuring one of these variables (q_w)
182 and two variables that directly respond to changes in these variables (C_s and D_s), it is pos-
183 sible to constrain the state of the transport system and predict unknown variables including
184 bedload flux. In this manner, C_s and D_s are viewed as proxies for S and D_b .

185 As an aside, equation (1) can also be derived by combining simplified relations pre-
186 sented in the canonical sediment transport literature [e.g. Wong & Parker, 2006; Engelund
187 & Hansen, 1967; Brownlie, 1983; Garcia & Parker, 1991]; however, many of these relations
188 have empirical origins and thus contain large, unquantifiable uncertainty. Rather than com-
189 bining a series of existing empirical expressions, we fit β_i parameters and quantify predictive
190 uncertainty directly; this approach minimizes predictive bias assuming that available data
191 sufficiently capture the underlying physical processes.

192 The majority of this paper focuses on the development and application of a statisti-
193 cal methodology used to estimate empirical scaling parameters in equation (1) and predict
194 bedload flux. We present an example application at our field site on the Colorado River in
195 Grand Canyon National Park, where estimates of bedload flux obtained from repeat bathy-
196 metric surveys of dune migration paired with concurrent gage measurements form the ob-
197 servational basis for statistical analyses. Parameter estimation and prediction is conducted
198 using Bayesian inference which facilitates consistent propagation of uncertainty from multi-
199 ple sources of information and prediction of distributions for quantities of interest [Schmelter
200 *et al.*, 2011; Schmelter & Stevens, 2012; Schmelter *et al.*, 2015]. This approach is particularly
201 useful for propagating uncertainty arising from both measurement uncertainty and parameter
202 estimation uncertainty in calculations of cumulative sediment load [Schmelter *et al.*, 2012].

203 In addition to the data from our site, we also consider data from six other rivers re-
204 ported by Toffaleti [1968] in order to test generality and improve the predictive power of our
205 model. These data cover a much wider range of discharge, slope, and bed grain size condi-
206 tions than those that are found at the site on the Colorado River. In order to incorporate these
207 data into the predictive model for bedload flux at our site, we consider three statistical mod-
208 els that are distinguished in principle by their assumptions regarding the universality of scal-
209 ing exponents and in practice by their treatment of groups in the data. These approaches have

210 advantages and disadvantages to each other relative to the specific modeling conditions and
 211 objectives, as well as the quantity and quality of data that are available at a site of interest.

212 3.2 Statistical methods

213 3.2.1 Bayesian linear regression

214 The generalized linear model given by equation (1) has four unknown parameters that
 215 must be estimated from a large number of observations of model variables. This system is
 216 overdetermined and no single solution can fit all of the data simultaneously. As a result, it is
 217 necessary to employ regression analysis to handle uncertainty and error. Log-transformed
 218 variables enable linear regression, which assumes that the i^{th} observation of the response
 219 variable $\log(q_b)_i$ can be expressed as a linear function of the predictor variables $\log(Q)_i$,
 220 $\log(C_s)_i$ and $\log(D_s)_i$, plus an error term ϵ_i

$$\log(q_b)_i = \log(A)_i + \beta_0 + \beta_1 \log(q_w)_i + \beta_2 \log(C_s)_i + \beta_3 \log(D_s)_i + \epsilon_i \quad (8)$$

221 Perhaps the most common variant of linear regression is Ordinary Least-Squares (OLS),
 222 which finds the combination of model parameters β_0 , β_1 , β_2 , and β_3 that minimizes the sum
 223 of the sum of the squared error terms. OLS regression leads to an unbiased predictor of the
 224 response variable assuming ϵ_i is normally distributed and independent across all samples.
 225 However, for the purposes of the present research, this approach has several limitations. OLS
 226 regression cannot handle hierarchical organizations of data that potentially violate the as-
 227 sumed independence of ϵ_i , such as when individual observations are grouped by river or site.
 228 Additionally, analytical quantification of predictive uncertainty in the OLS framework does
 229 not readily allow for propagation of errors through mass-balance calculations.

230 Bayesian inference provides a convenient framework for overcoming these issues.
 231 For a general discussion of Bayesian methods, see *Gelman et al.* [1995]; *Christensen et al.*
 232 [2011]. The standard Bayesian approach to linear regression starts with the same assump-
 233 tions as OLS that are encapsulated by (8). However, we introduce an additional parameter σ
 234 that quantifies the standard deviation of the error term, i.e.:

$$\epsilon_i \sim \mathcal{N}(0, \sigma) \quad (9)$$

235 where the tilde means “distributed as” and $\mathcal{N}(0, \sigma)$ is an independent normal distribution
 236 with zero mean and standard deviation σ . Consequently, we aim to draw inference on five
 237 parameters: β_0 , β_1 , β_2 , β_3 , and σ .

238 At this point we note for clarity that the term “variables” refers to measurable physical
 239 quantities, while the term “parameters” refers to unknown quantities that appear in the data
 240 model and are the object of statistical inference. Henceforth, we use θ to refer to the 5×1
 241 vector of model parameters, i.e. $\theta = [\beta_0, \beta_1, \beta_2, \beta_3, \sigma]$. Additionally, we use \mathbf{X} to refer to the
 242 $4 \times N$ matrix of N observations of model variables q_w , C_s , D_s , and q_b .

243 While OLS regression seeks estimates of model parameters that minimize the global
 244 sum of the squared residuals, Bayesian model fitting embraces uncertainty associated with
 245 the fact that small differences in model parameters may fit the data nearly as well as the op-
 246 timal result. These small differences are quantified by the likelihood function, which exists
 247 on the domain of model parameters assuming fixed observational data \mathbf{X} , and is denoted by
 248 $L(\theta|\mathbf{X})$. Here, the vertical line denotes conditional dependence, i.e. the likelihood of θ given
 249 \mathbf{X} . The likelihood can be computed for any combination of parameters, where higher like-
 250 lihoods represent more likely combinations of parameters. Introducing the prior probability
 251 distribution $P(\theta)$, we obtain an expression for the posterior probability distribution of model
 252 parameters conditional on observational data $P(\theta|\mathbf{X})$ through Bayes theorem:

$$P(\theta|\mathbf{X}) = \frac{L(\theta|\mathbf{X})P(\theta)}{\int L(\theta|\mathbf{X})P(\theta)d\theta} \quad (10)$$

253 Once the posterior probability distribution of model parameters is known, unobserved values
 254 of q_b can be estimated from measured values of predictor variables using Bayesian posterior
 255 predictive distributions, which efficiently propagate uncertainty through individual estimates
 256 of q_b as well as time-integrated mass-balance calculations.

257 **3.2.2 Grouped, ungrouped, and hierarchical model variations**

258 The basis for equation (1) suggests that it is sufficient to predict bedload flux in any
 259 sand bed river using a single universal set of scaling parameters. However, some degree of
 260 predictive uncertainty is inevitable owing to both measurement error and model bias arising
 261 from simplification of physical processes. While measurement error can be considered
 262 uncorrelated, systematic biases are caused by a failure of the data model to capture specific
 263 physical processes, and are thus likely to be correlated when conditions are similar. As a result,
 264 we anticipate persistent site-specific biases using a general model based on data from
 265 many rivers. For example, details of channel geometry not explained by width and slope may
 266 cause bedload flux to be more or less sensitive to changes in water discharge at one site compared
 267 with the central tendency of all sand bed rivers. In this case, better predictive accuracy
 268 would be achieved at that site by adjusting the value of β_1 to reflect this difference. In general,
 269 we anticipate better predictive performance if model parameters are constrained on a
 270 site-specific basis.

271 This theoretical consideration is at odds with practical limitations: regression analysis
 272 requires numerous independent estimates of bedload flux that are expensive and difficult to
 273 obtain. Thus, it would be advantageous if existing data from many rivers could be used to
 274 help inform bedload prediction at a new site. Optimal model parameters may differ slightly
 275 from site to site; however, sand-bed rivers are all governed by the same general physical processes
 276 such that it is reasonable to expect that scaling parameters should be similar between
 277 rivers. In order to balance theoretical and practical concerns, we consider three distinct generative
 278 data models, each of which reflects a different trade-off between observational data requirements
 279 and assumptions regarding the generality of scaling parameters.

280 The first model (the grouped model, Appendix B.1) assumes a single universal set of
 281 model parameters $\theta = [\beta_0, \beta_1, \beta_2, \beta_3, \sigma]$. The standard deviation of the error term σ is the
 282 same for all data. All observations are therefore treated as independent observations from
 283 the same exchangeable group of observations. The advantage of this model is that it can be
 284 applied at a new site without collecting any additional data. However, it ignores the possibility
 285 of correlated errors by river or site, and is therefore subject to unquantifiable systematic
 286 biases when applied at a specific site without local data.

287 The second model (the ungrouped model, Appendix B.2) assigns different independent
 288 scaling parameters $\theta_j = [\beta_{j0}, \beta_{j1}, \beta_{j2}, \beta_{j3}, \sigma_j]$, for $j = 1, \dots, m$ and $m = 8$ is the number
 289 of data groups (i.e. independent sites). This is equivalent to performing grouped regression
 290 independently on a site-specific basis: each site is treated as an independent statistical entity
 291 comprising its own exchangeable group of observations. This model is perhaps the most theoretically
 292 conservative in that it assumes nothing with regard to physical similarity between
 293 sites. However, it is also the least practical in that it requires extensive uncorrelated observations
 294 of bedload flux from each monitoring site in order to ensure reliable results, and cannot
 295 be applied at a site where bedload has never been measured directly.

296 The third model (the hierarchical model, Appendix B.3) assigns different regression
 297 coefficients to each site, but assumes some degree of physical similarity between sites. Observations
 298 are treated as exchangeable on a site-specific basis, and each site comes from an exchangeable
 299 group of sites, that is, all sand bed rivers. We aim to draw inference, not only
 300 on the behavior of individual sites, but also on the distribution of behaviors that can be observed
 301 at different sites. Site-specific coefficients are thus determined partly by data collected
 302 at that site, but are also informed by the behavior of other rivers which can reduce issues related
 303 to low sample size at one site if sufficient data exists at other sites. Hierarchical organ-

304 ization is implemented through priors for the regression coefficients which are assumed to
 305 be normally distributed with a mean and variance that reflects the central tendency and vari-
 306 ability of sand-bed rivers. This model lies somewhere between the grouped and ungrouped
 307 models in terms of both theoretical assumptions and data requirements. Some data are use-
 308 ful in order to constrain bedload flux at a new site, but limited observations are utilized to
 309 greater effect than in the ungrouped model.

310 **3.2.3 Priors**

311 Diffuse (i.e. wide, minimally informative) priors are commonly used to minimize in-
 312 fluence on model results, and are employed here for all three model variations. Diffuse priors
 313 are effectively constant over the relevant parameter domain, which means that the posterior
 314 distribution is essentially reflects a renormalization of the likelihood function, preserving
 315 the relative log-likelihoods while ensuring the posterior integrates to 1. Due to the relatively
 316 large sample size, our results are not sensitive to the specific choice of diffuse prior.

317 Grouped and ungrouped regression models were fit using an approximation for Jef-
 318 frey’s prior, which is an attractive choice due its unique theoretical properties [*Gelman et*
 319 *al.*, 1995; *Christensen et al.*, 2011]]. Jeffrey’s prior is a uniform distribution on the domain
 320 $(\beta_0, \beta_1, \beta_2, \beta_3, \log(\sigma))$, which is an improper prior because it does not integrate to 1. Thus,
 321 normal distributions centered on zero with large standard deviations are used to approximate
 322 Jeffrey’s prior because a normal distribution approaches a uniform distribution as the stan-
 323 dard deviation goes to infinity. Jeffrey’s prior is also uniform $\log(\sigma)$ meaning the prior prob-
 324 ability that the parameter is between 0.01 and 0.1 is the same as the probability the parameter
 325 is between 0.1 and 1. The inverse gamma distribution approaches a uniform distribution on
 326 $\log(\sigma)$ as its parameters go to zero.

327 The hierarchical model structure is implemented through informative, dynamic pri-
 328 ors, where the parameters for these priors are referred to as “hyperparameters”. Inference
 329 is drawn on parameters and hyperparameters simultaneously such that the hyperparameters
 330 have their own prior and posterior probability distributions. Priors for hyperparameters, or
 331 “hyperpriors” must be specified. Again, we utilized diffuse, minimally-informative hyperpri-
 332 ors, the specific choice of which does not influence model results. For additional details on
 333 priors and hyperpriors, see Appendices B.1, B.2, and B.3.

334 **3.2.4 Model fitting**

335 All three models were fit using Markov Chain Monte-Carlo (MCMC) sampling meth-
 336 ods. This technique is commonly used to sample the posterior distribution and conduct pre-
 337 dictive simulation when analytical alternatives are cumbersome or impossible. For additional
 338 details on MCMC sampling, see Appendix B.4 and example workflows [*Ashley*, 2019b].

339 **3.2.5 Model selection**

340 Quantitative comparison of predictive power is accomplished using the Deviance Infor-
 341 mation Criterion (DIC, *Spiegelhalter et al.* [2002]; *Gelman et al.* [2014]), Appendix B.6), a
 342 generalization of the Akaike Information Criterion that is suitable for comparing the hierar-
 343 chical and non-hierarchical models used here. DIC includes two two terms: one which quan-
 344 tifies in-sample predictive accuracy and one which corrects for model complexity to approx-
 345 imate out-of-sample predictive accuracy under certain assumptions [*Gelman et al.*, 2014].
 346 As a relative measure of predictive power, models with lower DIC are expected to have lower
 347 prediction error than models with higher DIC. However, DIC is not a perfect measure of rel-
 348 ative prediction error and is reported here (Table 2) to inform model evaluation rather than as
 349 the sole discriminatory factor.

3.3 Field methods

Transport-related data were collected at one field site on the Colorado River in Grand Canyon National Park during three field campaigns in the Spring and Summer of 2015, as well as the Fall of 2016. The site (Figure 2) is located at river mile 225 in the vicinity of USGS monitoring station 09404200 (Colorado River above Diamond Creek near Peach Springs, AZ). Hereafter, we refer to this site informally as "Diamond Creek" or the "Diamond Creek field site". Data include repeat bathymetric surveys of dune migration, ADCP surveys of flow velocity, suspended sediment and bed sediment samples, and bed photographs for optical grain-size analysis [Buscombe *et al.*, 2010]. Concurrent gage measurements of water discharge, suspended sand concentration, and grain size were also collected following standard procedures during this time [Rantz *et al.*, 1982; Topping & Wright, 2016].

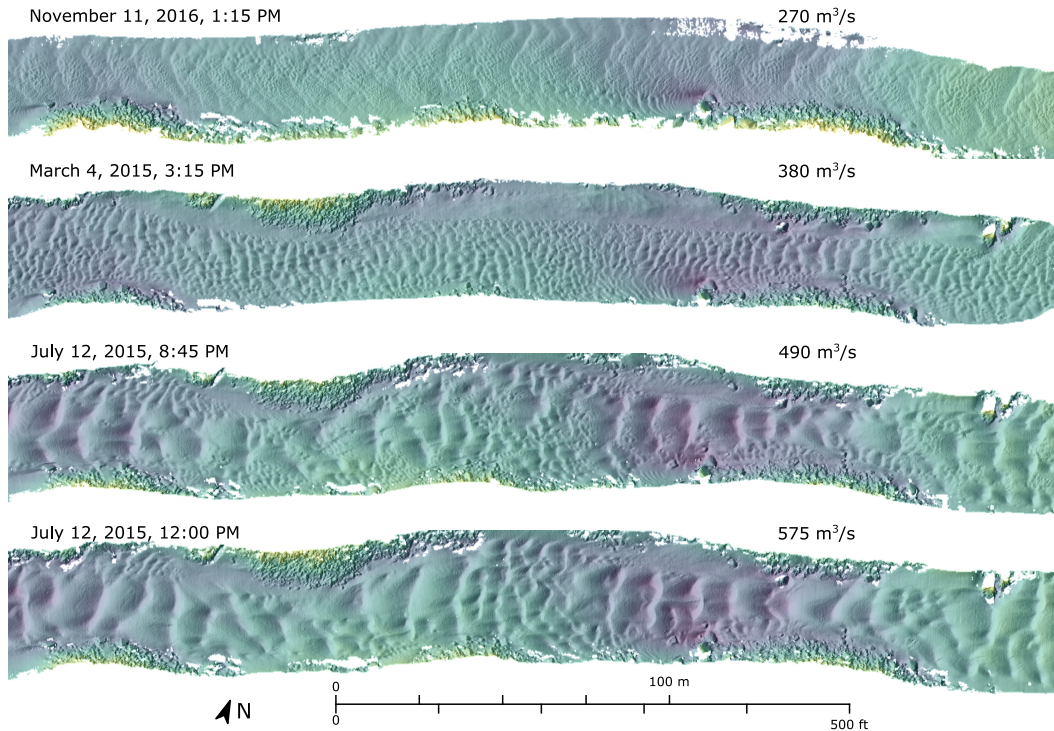
Estimates of bedload flux were obtained using 320 high resolution, full-width bathymetric surveys of an approximately 400 meter reach adjacent to the Diamond Creek gaging station. Surveys were collected using a 400 kHz Reson 7125 multibeam echo sounder (MBES) which produces a swath comprised of 512 beams (each 1 x 0.5 degrees) across a transverse subtended angle of 135 degrees. In order to map sonar returns onto a global coordinate system, the location of the boat was tracked using a robotic Total Station referenced to a fixed position on the bank, and a fiber-optic gyrocompass and inertial sensors were used to calculate heading, roll, and pitch of the sonar head. Patch tests were conducted before the surveys to determine the offset angles and timing latency between the various system components. Bad soundings and sweep misalignments (due to, for example, systematic side-lobe interference; and scattering of soundings by air bubbles, drifting insects and other organic matter in the water) were identified by manual sweep editing and systematically stepping through overlapping sweeps. Quality assurance assessments were performed after the surveys by comparing selected soundings from all surveys over a large, flat-topped rock located along the channel margin. The mean standard deviation of soundings over this feature was 0.015 m and indicate a high level of survey precision. The final, edited surveys used here are ungridded point clouds, where each point corresponds to a valid sonar return from the river bed. More details about acquisition of MBES data with this instrument and configuration are found in Kaplinski *et al.* [2009]; Kaplinski *et al.* [2014], Grams *et al.* [2013, 2018], and Buscombe *et al.* [2014a,b]. Four example surveys are plotted in Figure 3.

Simons *et al.* [1965] provide the method by which bathymetric data can be used to generate bedload flux estimates. Their expression is given by:

$$q_b = (1 - p)V_c \frac{H_c}{2} + C, \quad (11)$$

where q_b [L^2T^{-1}] is the volumetric bedload flux per unit width, p [-] is the bed porosity taken to be a constant 0.35, V_c [LT^{-1}] is a characteristic bedform migration rate, H_c [L] is a characteristic bedform height, and C is a constant of integration assumed to be zero. Measured bedform heights ranged from 0.15 to 0.70 m, and measured migration rates ranged from 0.21 to 1.76 m/hr. Both of these quantities varied predictably with water discharge.

Equation (11) is derived from a statement of mass conservation (the Exner equation, Paola & Voller [2005]) combined with a simplified model for dune evolution characterized by translationally invariant migration of triangular or sinusoidal forms. Although it represents substantial simplifications of physical process (for example, by ignoring bedform deformation and variability in bedform migration rate and geometry), flume and field studies find good agreement between (11) and other estimates of bedload flux across a wide range of conditions extending from the threshold of bedform development to suspension-dominated dunes [Simons *et al.*, 1965; Engel & Lau, 1980; van den Berg, 1987; Mohrig & Smith, 1996]. Consequently, we argue that this expression provides a reasonable estimate of bedload transport that is not captured by acoustic estimates of suspended sand load. Equation (11) was used to compute 55 hourly estimates of average bedload flux (Figure 4). Major elements of



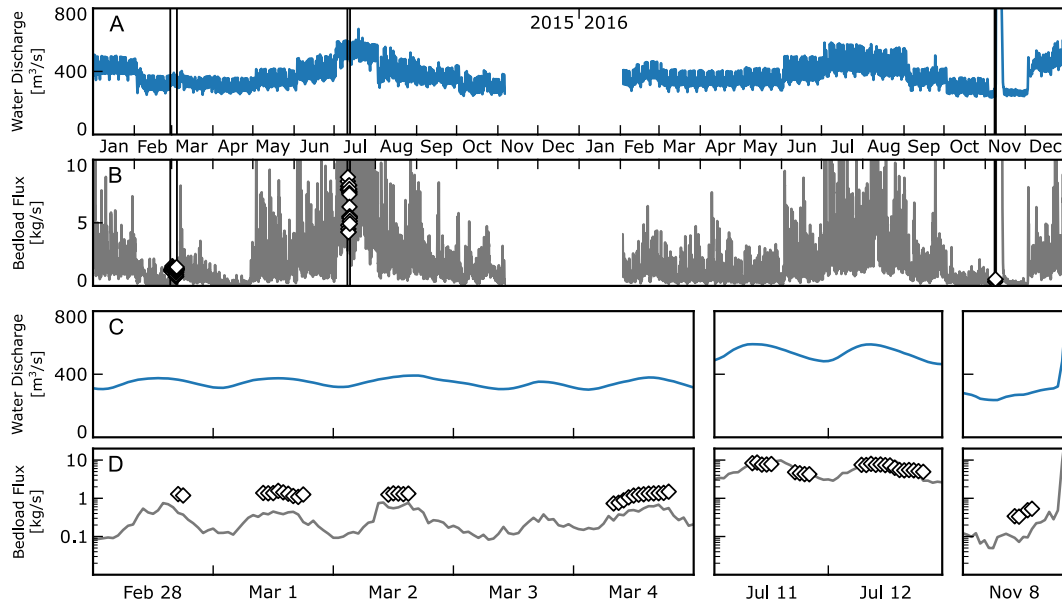
381 **Figure 3.** Example bathymetric surveys with shaded relief plotted at 10 cm resolution. Water discharge dur-
 382 ing the survey is indicated in the upper right corner of each survey. Flow is from right to left. Colors represent
 383 water depth, as in figure 2.

402 this procedure are discussed in Appendix A. Additional details can be found in the documen-
 403 tation of software developed for this purpose [Ashley, 2019a]

408 3.4 Additional data from other rivers

409 The large river dataset presented by *Toffaletti* [1968] (and derived quantities) is used to
 410 supplement limited data from our field site. This dataset comprises a total of 262 concurrent
 411 observations of bedload flux Q_b , water discharge Q_w , suspended sand concentration C_s , me-
 412 dian suspended sand diameter D_s , and channel width W on the Atchafalaya River ($n = 60$),
 413 the Mississippi River in Louisiana ($n = 47$), the Mississippi River in Missouri ($n = 63$),
 414 the Red River ($n = 28$), the Rio Grand River ($n = 36$), the Middle Loup River ($n = 9$),
 415 and the Niobrara River ($n = 19$). These sites are similar to the Diamond Creek field site in
 416 that the predominant bed material is sand; however they are different in that they are all al-
 417 luvial rivers (whereas the Colorado River in Grand Canyon is a bedrock-confined alluvial
 418 river with gravelly and sandy reaches). Our model is based on physical theory describing
 419 one-dimensional transport, and assumes nothing about channel form. Consequently, it can be
 420 applied in rivers that are not fully alluvial as long as the bed material at the site of interest is
 421 sand.

422 Total suspended sand concentration C_s and median suspended sand grain size D_s were
 423 computed from reported grain-size specific suspended sediment concentrations. Bedload
 424 flux was computed according to the revised Meyer-Peter & Müller bedload equation [Wong
 425 & Parker, 2006] with grain stresses estimated using the Einstein drag partition as reformu-
 426 lated by *Garcia* [2008]. This procedure was also used to compute bedload flux at our study
 427 site when flow velocity and bed sediment data are available to check approximate correspon-



404 **Figure 4.** Time series plot of water discharge (A) and bedload flux (B) at the Diamond Creek sediment
 405 monitoring station in 2015 and 2016. Grey line shows bedload flux estimated as a constant fraction (5%) of
 406 suspended load, and black diamond show hourly average estimates of bedload flux from bedform migration.
 407 Insets (C, D) highlight the periods where bedform flux estimates are available.

428 dependence with estimates of flux from dune migration. Note that here, and throughout, “observations”
 429 is used as part of the statistical vernacular to refer to independent samples of variables
 430 and implies nothing about how those samples were obtained. This distinction is particularly
 431 important here because “observations” of bedload flux are actually computed from depth,
 432 slope, grain size, and flow velocity using physically-based model. Similarly, observations
 433 of bedload flux at Diamond Creek are computed using a physically-based model from dune
 434 height and velocity.

436 3.5 Data treatment

437 The statistical methods employed here assume errors in observations are uncorrelated.
 438 However, the 55 hourly estimates of average bedload flux from the Diamond Creek field site
 439 were collected over seven days during which temporal correlation is likely. Unqualified ex-
 440 trapolation of trends in this dataset to the full gage record spanning nearly ten years may
 441 therefore produce unrealistic results. In order to mitigate this effect, we use only the first and
 442 last measurement from each day ($n = 14$) in order to estimate model parameters.

443 The full data set used for statistical analysis comprises a total of 276 observations from
 444 eight sites. Data were log-transformed to obtain the linear regression variables q_w^* , C_s^* , D_s^* ,
 445 and q_b^* using fixed reference values of each variable (Figure 5). We chose to use a single
 446 reference values for each variable (as opposed to individual reference values for each site)
 447 computed as the geometric mean of all 276 pooled observations of each variable, which re-
 448 sults in centered (zero mean) log-transformed variables. Other choices may provide addi-
 449 tional insight (if for example, different physically important reference values are used on a
 450 site-specific basis like mean annual discharge or bankfull discharge); however, such anal-
 451 yses are beyond the scope of this paper. Reference values of model variables are given by:
 452 $q_{b0} = 0.039$ kg/s/m, $q_{w0} = 4.35$ m²/s, $C_{s0} = 1.07 \times 10^{-4}$, and $D_{s0} = 0.13$ mm. Chan-

435

Table 1. Summary of variable ranges measured at each site

	Q_w [m^3/s]		W [m]		$\log_{10}(S)$		D_b [mm]	
	min	max	min	max	min	max	min	max
Atchafalaya River	931	14186	314	503	-5.0	-4.3	0.10	0.41
Mississippi @ Tarbert Landing	4248	28827	896	1414	-4.7	-4.4	0.20	0.38
Mississippi @ St. Louis	1512	8778	457	518	-5.0	-3.2	0.20	0.86
Red River	190	2826	130	183	-4.2	-3.1	0.11	0.28
Rio Grande River	35	286	41	198	-3.1	-3.0	0.25	0.45
Middle Loup River	9	14	22	46	-2.9	-2.7	0.34	0.48
Niobrara River	6	21	19	41	-2.9	-2.7	0.30	0.40
Colorado @ Diamond Creek	267	590	59	64	-4.0	-3.7	0.30	0.50
	q_w [m^2/s]		C_s [ppm]		D_s [mm]		Q_b [kg/s]	
	min	max	min	max	min	max	min	max
Atchafalaya River	2.9	28.6	4	372	0.08	0.16	0.20	12.5
Mississippi @ Tarbert Landing	4.7	24.2	5	199	0.10	0.18	0.43	6.7
Mississippi @ St. Louis	3.3	17.2	13	307	0.10	0.25	0.63	11.6
Red River	1.2	20.1	8	495	0.09	0.12	0.10	3.3
Rio Grande River	0.3	3.4	373	3177	0.12	0.22	1.5	41.1
Middle Loup River	0.2	0.6	183	1032	0.13	0.18	1.8	7.8
Niobrara River	0.2	0.9	189	1088	0.08	0.18	1.0	11.0
Colorado @ Diamond Creek	4.5	9.1	2	135	0.12	0.22	0.33	8.6

453 nel widths were computed using an empirical power-law function of water discharge at the
 454 Diamond Creek field site. Reported widths were used at other sites.

455 Here, we emphasize that the full dataset contains observations of bedload flux that
 456 were obtained using two very different methods. Bedload was estimated from grain stresses
 457 computed using the Einstein drag partition and the Wong & Parker bedload equation for the
 458 large river dataset reported by *Toffaletti* [1968], while bedload flux at Diamond Creek was
 459 computed using observations of bedform migration. For the purposes of statistical analysis,
 460 we assume both methods produce unbiased estimates of bedload flux with comparable un-
 461 certainty. Consequently, both methods are treated identically in the context of inference and
 462 prediction.

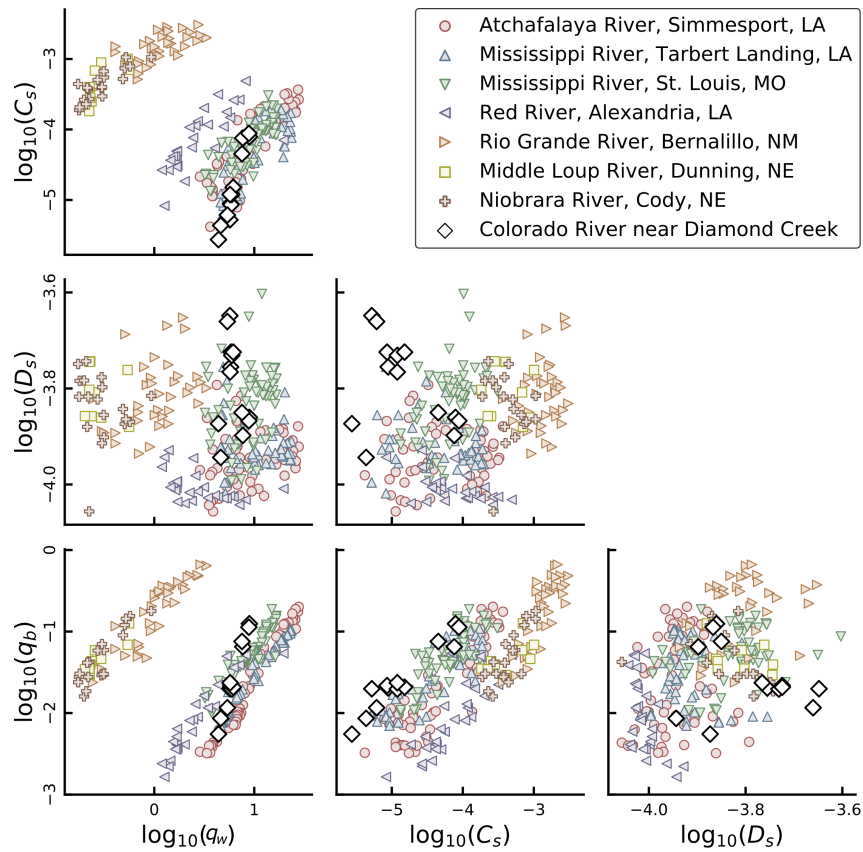
467 4 Results

468 4.1 Bedload fluxes at Diamond Creek

469 Bedload flux computed from bedform migration is similar to bedload flux estimated as
 470 a constant 5% of suspended sand load during the July 2015 survey period, corresponding to
 471 the highest water discharges observed (450 m^3/s to 600 m^3/s). Bedload fractions are signif-
 472 icantly higher during the March 2015 and November 2016 survey periods, corresponding to
 473 lower water discharges (275 m^3/s to 400 m^3/s). Bedload flux ranged from 0.33 kg/s to 8.6
 474 kg/s during the various data collection intervals (Figure 4). The bedload fraction is nega-
 475 tively correlated with suspended sand flux, ranging from as little as 3% to as much as 26% of
 476 suspended sand flux.

477 4.2 Inference on model parameters

478 Kernel density estimates of the marginal posterior distributions of model parameters
 479 are plotted in Figure (6). The statistical effect of each predictor variable is quantified by
 480 the value of the β exponent corresponding to that variable. Peaked distributions indicate low



463 **Figure 5.** Expanded visualization of regression data. Pale colored markers indicate values of model vari-
 464 ables computed from data reported by *Toffaletti* [1968]. Note that predictor variables (q_w , C_S and D_S) cover a
 465 wide range of conditions and are only weakly correlated when viewed collectively. Site-specific correlations
 466 are evident, especially between C_S and q_w

492

Table 2. Median posterior parameter estimates

Location	β_0	β_1	β_2	β_3	σ
Grouped Model (DIC = 552)					
All	0.08	0.048	0.68	1.65	0.52
Ungrouped Model (DIC = 382)					
Atchafalaya River	-1.68	1.65	0.21	-0.24	0.20
Mississippi @ Tarbert Landing	-1.41	1.39	0.09	-0.27	0.16
Mississippi @ St. Louis	-0.58	1.29	0.11	0.02	0.25
Red River	-0.90	1.01	0.41	-0.18	0.24
Rio Grande River	1.07	0.92	0.68	0.01	0.34
Middle Loup River	2.95	0.95	0.02	-0.96	0.26
Niobrara River	2.84	1.08	0.27	-1.10	0.32
Colorado @ Diamond Creek	-2.56	5.04	-0.16	-0.35	0.10
Hierarchical Model (DIC = 123)					
Atchafalaya River	-1.63	1.61	0.22	-0.19	0.22
Mississippi @ Tarbert Landing	-1.35	1.36	0.11	-0.20	0.22
Mississippi @ St. Louis	-0.51	1.24	0.15	-0.16	0.22
Red River	-0.90	1.04	0.39	-0.19	0.22
Rio Grande River	1.47	1.01	0.57	-0.16	0.22
Middle Loup River	2.45	0.87	0.14	-0.22	0.22
Niobrara River	2.68	1.07	0.31	-0.30	0.22
Colorado @ Diamond Creek	-0.43	2.07	0.36	-0.12	0.22
μ_k	0.19	1.30	0.28	-0.21	
σ_k	1.83	0.44	0.18	0.11	

parameter estimation uncertainty, and wide distributions indicate high uncertainty. Median parameter estimates are reported in Table 2.

Computed DIC values indicate that the hierarchical model has the lowest expected prediction error averaged across all sites. In order to evaluate the effect of each parameter on predictive power, we computed DIC using permutations of each model involving only two predictor variables. The predictive power using the grouped model is significantly reduced using any of the two-variable permutations. However, we find that the predictive power of the ungrouped model is improved by ignoring D_s^* (DIC = 298 compared to 382). This indicates that considering D_s^* does not improve model fit enough to justify the added complexity. Excluding D_s^* has essentially no effect on the predictive power of the hierarchical model (DIC = 112 compared to 123).

4.3 Prediction

Predictive distributions of total mass bedload flux (Appendix B.5) were computed using all three models using hourly-average measurements of Q , C_s , and D_s recorded at the Diamond Creek gage from January 1, 2008 to December 31, 2016. This was accomplished by computing full posterior predictive distributions for each gage measurement of model variables. Median predictions are compared against observational data in Figure (7). The full simulated time series of bedload flux, the ratio of bedload to suspended load, and predictor variables are plotted in Figure (8).

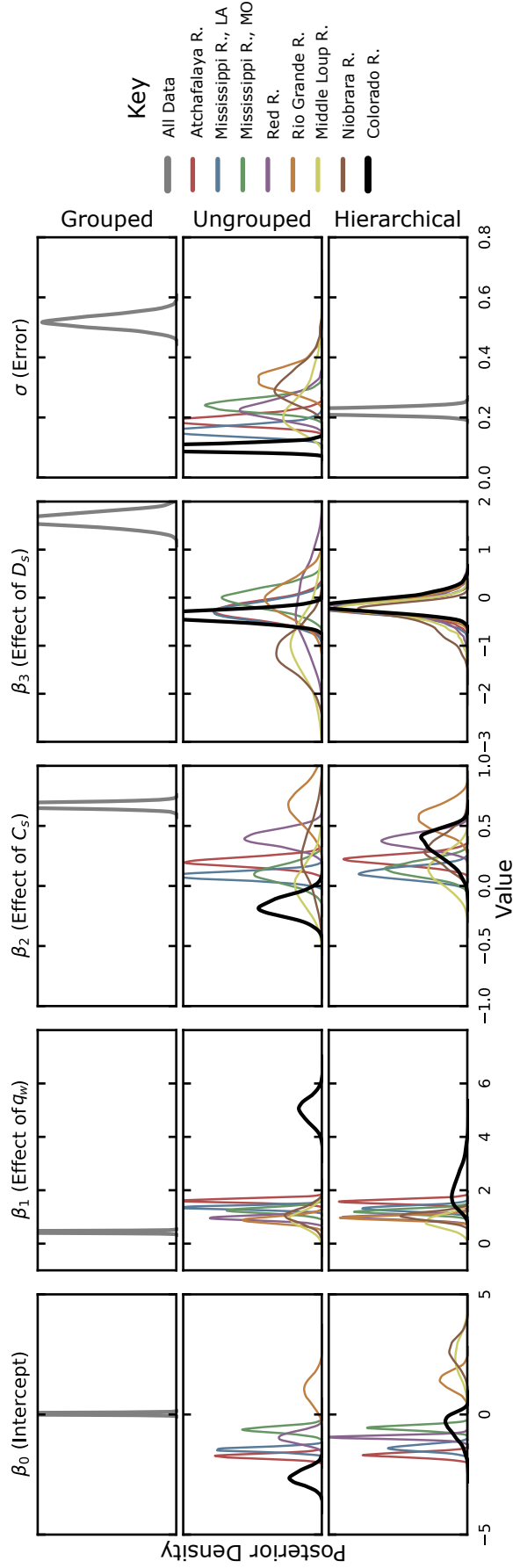
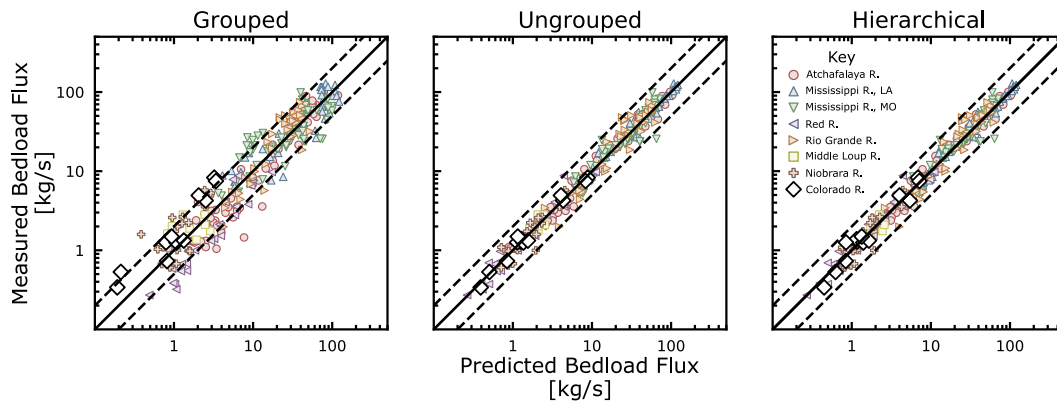
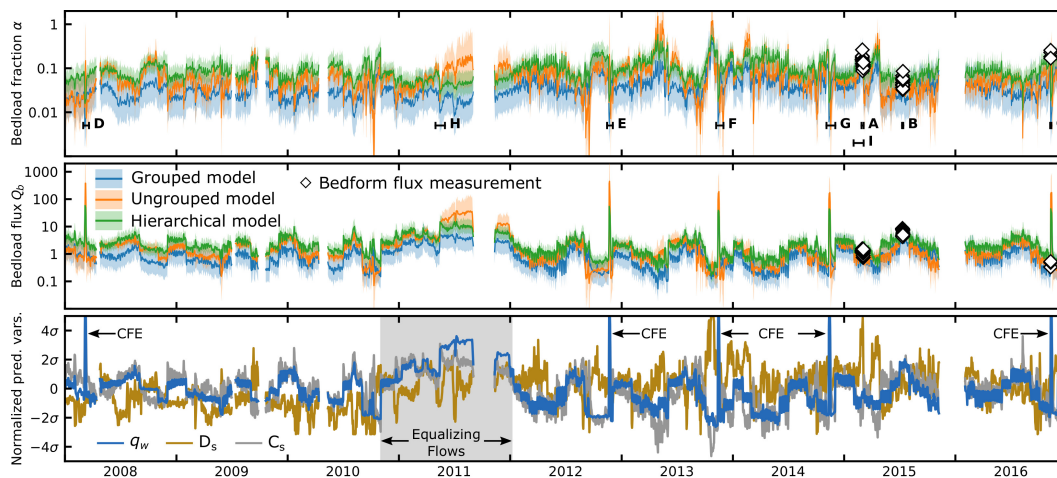


Figure 6. Marginal posterior distributions for model parameters. Distribution widths indicate parameter estimation uncertainty. The grouped model uses a single set of parameters to describe all data, while ungrouped and hierarchical model variations involve fitting separate regression parameters to each site. Note that site-specific posterior distributions are more clustered for the hierarchical model than for the ungrouped model owing to the dynamic, informative priors for the regression coefficients.



501 **Figure 7.** Plot comparing predicted and observed bedload flux. Predictions reflect median parameter estimates.
 502 estimates. Dashed lines indicate a factor of two deviation between predicted and observed bedload flux. Note
 503 that the ungrouped and hierarchical models provide improved fit compared with the grouped model. The
 504 hierarchical model leads to more precise estimates of model parameters while providing similar fit to the data
 505 when compared with the ungrouped model.



506 **Figure 8.** Simulated hourly-averaged bedload fraction (upper panel), bedload flux (middle panel) and
 507 transformed predictor variables (lower panel) over the full gage record. Dark lines represent the median of
 508 the predictive distribution for bedload flux. Shaded regions represent 95% prediction intervals. Bracketed
 509 segments denoted A through I are plotted in Figures (9), (10), and (11). Plotted predictor variables are log-
 510 transformed and then normalized by subtracting the mean and dividing by the standard deviation. Controlled
 511 flood experiments (CFE's) and elevated "equalizing flows" used to balance reservoir levels are also indicated
 512 in the bottom panel.

5 Discussion

5.1 Comparison of model variations

We have presented three variations on our generalized bedload modeling framework that differ in their assumptions, implementation, and interpretation. Here, we compare model variations in the context of the statistical inference and predictions reported in Section 4.

The grouped model most closely encapsulates the physical reasoning presented in Section 3.1, which argues that quasi-universal relationships between transport parameters emerge through the processes governing their interaction and equilibration. These relationships comprise three primary modes of variability driven by water discharge, channel geometry, and bed composition. Three predictor variables improve predictive power compared with any two-parameter model permutation, indicating that all three modes of variability are represented in the data.

In principle, the grouped model can be applied at any site to predict bedload flux, including new sites that lack direct observational data. However, while individual predictions are unbiased relative to the full dataset, systematic biases exist among groups of measurements that come from a single site; for example, the grouped model under-predicts bedload flux at the Diamond Creek field site (Figure 7). Systematic biases are problematic when computing sediment budgets because they accumulate over time to cause compounded errors.

By considering each site separately, the ungrouped and hierarchical models reduce site-specific systematic biases. They also reflect a restricted scope of physical process: while the grouped model represents quasi-universal physical relationships across many sites, the ungrouped and hierarchical models capture site-specific associations between variables. As a result, we find that two-parameter permutations of the grouped and hierarchical models (ignoring D_s) provide equal or better predictive power than the generalized three-parameter approach. This observation can be explained by the fact that slope is effectively fixed at each site over human timescales in comparison to the differences observed between rivers, reducing the number of principle modes of variability to two. These modes are driven by fluctuations in flow strength and sediment supply, where sediment supply influences fluxes through both “grain size and reach-geometric effects” (*sensu Topping et al. [2000a,b]*). This finding is potentially valuable for sediment monitoring purposes because measurements of C_s are significantly easier to obtain than measurements of D_s . C_s varies by many orders of magnitude and can be measured accurately using single-frequency instruments in a wide range of conditions, while D_s requires well sorted suspended material, two-frequency instrumentation, and is only accurate for a small range of grain sizes [*Topping & Wright, 2016*].

The hierarchical model differs from the ungrouped model in that the site-specific associations between variables are assumed to be similar between sites. Through this assumption, sites with many observations inform prediction at sites with relatively few observations. This effect is most clear at our field site, where few observations ($n = 14$) lead to spurious point estimates of regression parameters (Table 2) and large uncertainty (Figure 6) using the ungrouped model. The hierarchical model produces a slightly poorer fit to the data but yields much more precise and consistent estimates of regression parameters.

In summary, each model has a specific set of assumptions, data requirements, and limitations that must be evaluated in order to be applied to a specific problem. The grouped model reflects quasi-universal physical relationships between variables and can be applied at any site without training data but introduces systematic bias to cumulative bedload estimates. The ungrouped model minimizes site-specific, systematic biases and assumes nothing about similarity between sites but requires extensive observational data to be applied at a given site. The hierarchical model reduces the number of observations needed at a site relative to the ungrouped model under the assumption that sites are similar. Grouped and hierarchical models can potentially be applied using only measurements of Q_w and C_s .

Presently, we aim to compute sediment budgets over the full gage record at the Diamond Creek sediment monitoring station. We argue that the hierarchical model is the best choice for this purpose because it reduces systematic bias but provides efficient use of limited data. Time series predictions made using the hierarchical model are plotted over select intervals in Figures (9), (10), and (11).

5.2 Comparison with existing methods for estimating bedload flux

Prior to this research, the two primary methods for estimating bedload flux from gage data in practical applications are (1) rating curves with discharge [e.g., *Leopold & Maddock, 1953; Emmett & Wolman, 2001*] and (2) constant bedload coefficients based on continuous measurements of C_s [e.g., *Rubin et al., 2001; Grams et al., 2013*]. To highlight the advantages of the model presented here, we compare simulated bedload time series with rating curve and bedload coefficient predictions. Several short example intervals were selected for this purpose and are plotted in Figures (10) and (11).

Both approaches are special cases of our general model (equation 1), wherein certain parameters are fixed. For example, rating curves express bedload flux as a power-law function of water discharge, i.e.:

$$Q_b = kQ_w^m \quad (12)$$

which is similar to equation (1) with null coefficients on suspended sand concentration C_s and diameter D_s :

$$q_b = Ae^{\beta_0} q_w^{\beta_1} C_s^0 D_s^0 W^{1-\beta_1}. \quad (13)$$

Assuming width scales with discharge ($W = aQ_w^b$), this reduces to

$$Q_b = (Ae^{\beta_0} a^{1-\beta_1}) Q_w^{\beta_1 + b(1-\beta_1)}. \quad (14)$$

Here, $k = Ae^{\beta_0} a^{1-\beta_1}$ and $m = \beta_1 + b(1 - \beta_1)$ are assumed to be constant. For the purposes of comparing rating curve and hierarchical predictions, rating curve parameters (k and m) were found using ordinary least-squares regression applied to concurrent observations of water discharge and bedload flux obtained at the gaging station and from repeat surveys of dune migration, respectively. By specifying $\beta_2 = 0$ and $\beta_3 = 0$, rating curves assume a unique relationship between bed composition, channel geometry, and discharge, which is problematic because sediment supply limitation is known to modify the transport efficiency of a given discharge through reach-geometric and grain size effects [*Topping et al., 2000a,b*]. Sediment supply variability can thus cause systematic deviations from rating-curve predictions; pulses of fine bed material result in an enriched state characterized by increased bedload flux. Subsequent preferential evacuation of fine material produces a depleted state during which bedload flux is suppressed relative to a hypothetical discharge rating curve prediction (Figure 12). Our modeling approach provides the potential to capture the effects of sediment supply limitation parameterized by C_s and D_s . As a result, we interpret the difference between hierarchical model predictions and rating curve predictions as an indicator of the relative supply-limitation state of the Diamond Creek sediment monitoring reach: a positive difference is indicative of relative enrichment of fine sand whereas a negative difference is indicative of relative depletion.

Such enrichments or depletions are particularly pronounced during and after controlled flood experiments (Figure 10). For example, the period following each controlled flood typically records finer suspended sand grain sizes and elevated suspended sand concentrations relative to antecedent conditions, indicating fine-sediment enrichment [*Rubin & Topping, 2001*]. This is perhaps caused by delivery of fine material accessed above the typical high water line and/or the reworking of existing alluvial deposits in a manner that increases transport efficiency. Hierarchical model predictions are correspondingly elevated relative to rating curve predictions following each controlled flood.

Bedload coefficients are sometimes used to account for the contribution of bedload to total load in scenarios where measurements of suspended flux are available and bedload

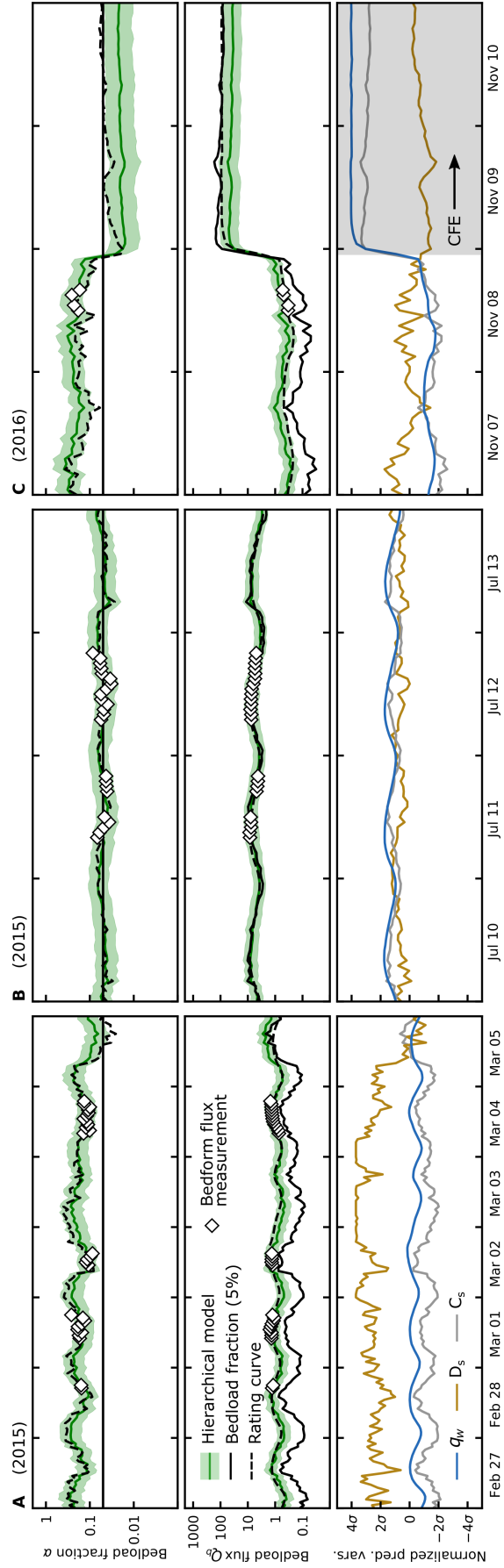


Figure 9. Simulated bedload fraction (upper panel), bedload flux (middle panel) and predictor variables (lower panel) at fifteen-minute resolution during the periods where observations of bedload flux from bedform migration are available. Plotted predictor variables are log-transformed and then normalized by subtracting the mean and dividing by the standard deviation.

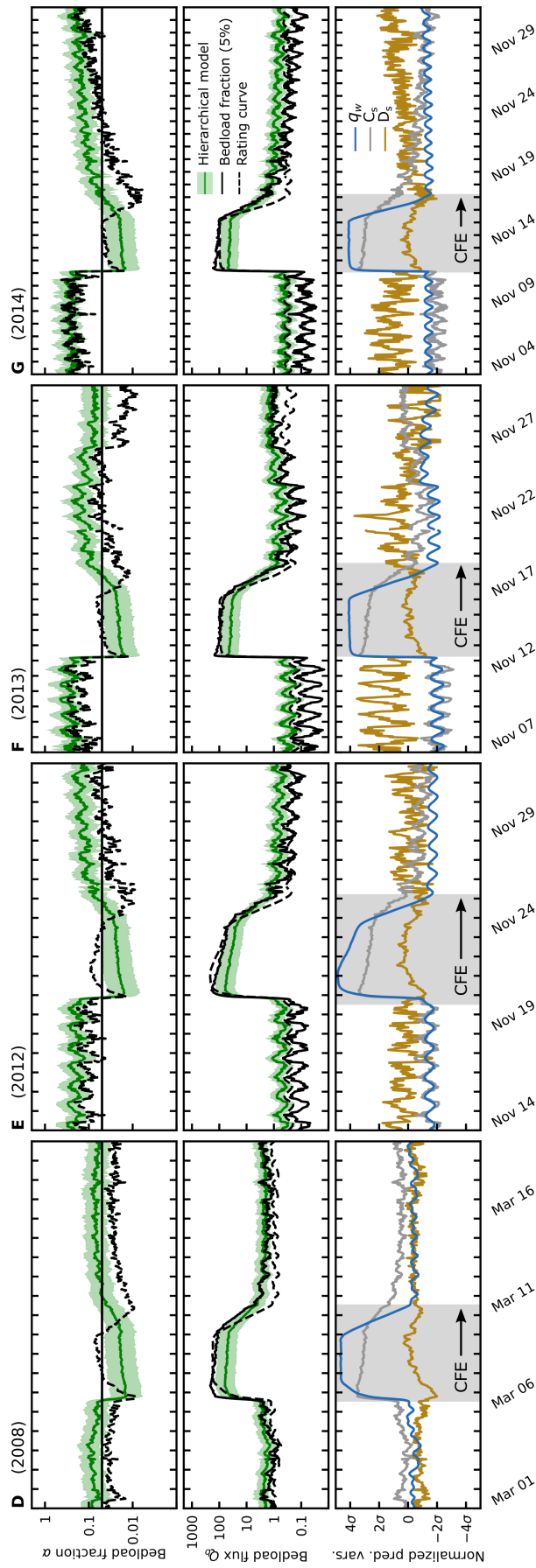


Figure 10. Simulated bedload fraction (upper panel), bedload flux (middle panel) and transformed predictor variables (lower panel) for the periods surrounding controlled flood experiments (CFEs).

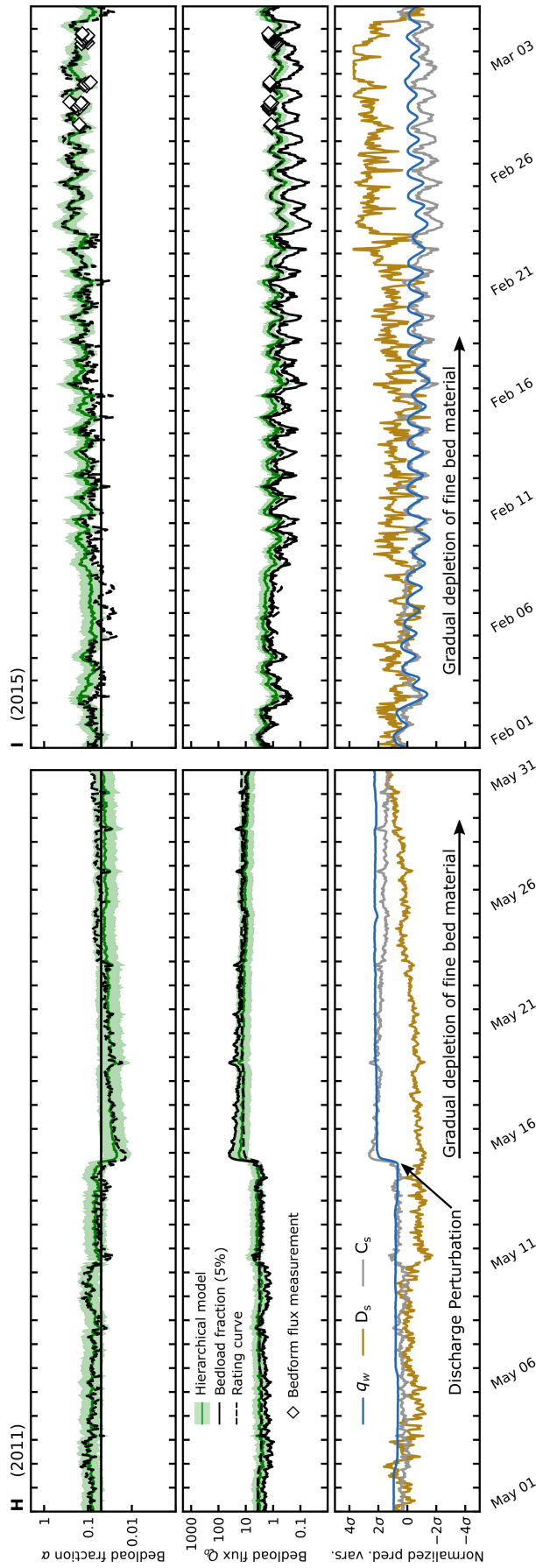
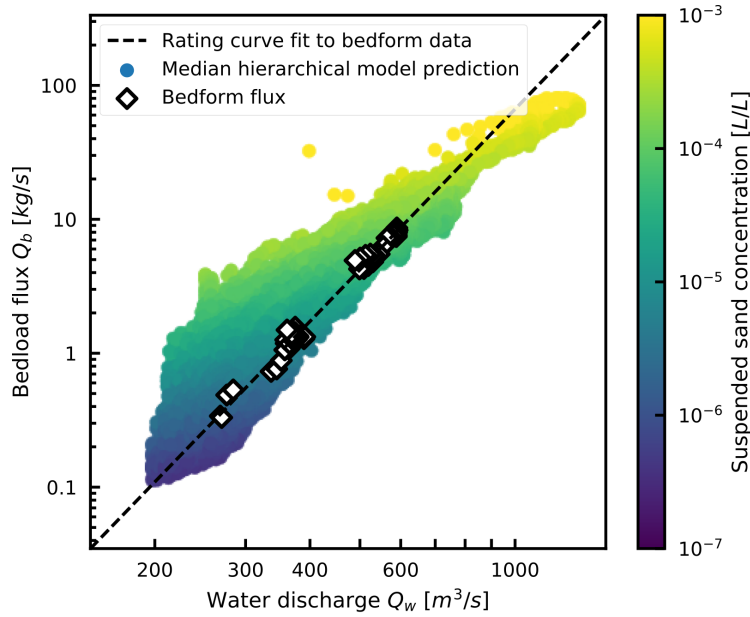


Figure 11. Simulated bedload fraction (upper panel), bedload flux (middle panel) and transformed predictor variables (lower panel) for two periods that record gradual coarsening of bed material under nearly constant (H) and periodically-fluctuating (I) flow conditions.



609 **Figure 12.** Plot illustrating the advantages of the proposed model over a traditional rating curve approach.
 610 Note that predicted bedload flux may vary by over an order of magnitude with respect to a fixed water dis-
 611 charge, an effect that is typically attributed to supply-limitation effects. Suspended sand concentration is
 612 connected to the supply-limitation state of a reach; here, elevated suspended sand concentrations indicative of
 613 fine-sediment enrichment and amplified bedload flux.

616 is thought to be small [e.g., *Grams et al.*, 2013]. In order to estimate total load, researchers
 617 sometimes apply a universal correction factor $1 + \alpha$ to measurements of suspended sand flux
 618 Q_s , which implies

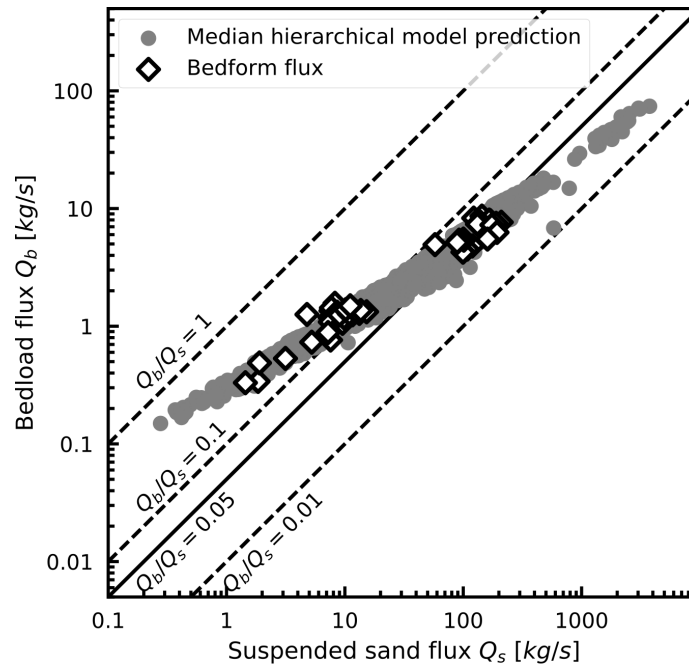
$$q_b = \alpha q_s. \quad (15)$$

619 Noting that $q_s = q_w C_s$, equation (15) is a special case of the our general bedload model (1)
 620 wherein $\beta_1 = 1$, $\beta_2 = 1$, and $\beta_3 = 0$, i.e.:

$$q_b = A e^{\beta_0} q_w^1 C_s^1 D_s^0. \quad (16)$$

621 Here, $\alpha = A e^{\beta_0}$ is the constant bedload coefficient. In some sense, this expression represents
 622 a crude attempt to account for supply limitation effects by assuming bedload and suspended
 623 load are equally sensitive to changes in their mutual causal predictors (water discharge, chan-
 624 nel geometry, and bed composition). However, suspension conditions (parameterized by the
 625 Rouse number, $Z_R = w_s / \kappa u_*$, where w_s is the particle settling velocity, u_* is the basal shear
 626 velocity, and κ is von Karman's constant) vary with flow strength and sediment supply, and
 627 are the most important predictor of α (*van Rijn* [1984], Equation 45). Insofar as the Rouse
 628 number may vary over time at a site, it is unreasonable to expect that the bedload fraction
 629 should remain constant. Instead, increasing Z_R should generally cause an increase in α . This
 630 may occur due to changes in u_* (as a function of water discharge, channel geometry, and bed
 631 roughness), or due to changes in w_s , which is a monotonically increasing function of D_b .

636 Comparison of hierarchical model and bedload coefficient predictions reveals sev-
 637 eral expected behaviors. In general, elevated suspended sand fluxes tend to correspond to
 638 increased suspension conditions (low Rouse numbers) and low bedload fractions (Figure 13).
 639 Bedload flux is a larger fraction of total load when discharge is low, corresponding to higher
 640 Rouse numbers due to decreases in u_* . Sediment supply depletion also increases the bed-
 641 load fraction when discharge is held constant, corresponding to higher Rouse numbers due to

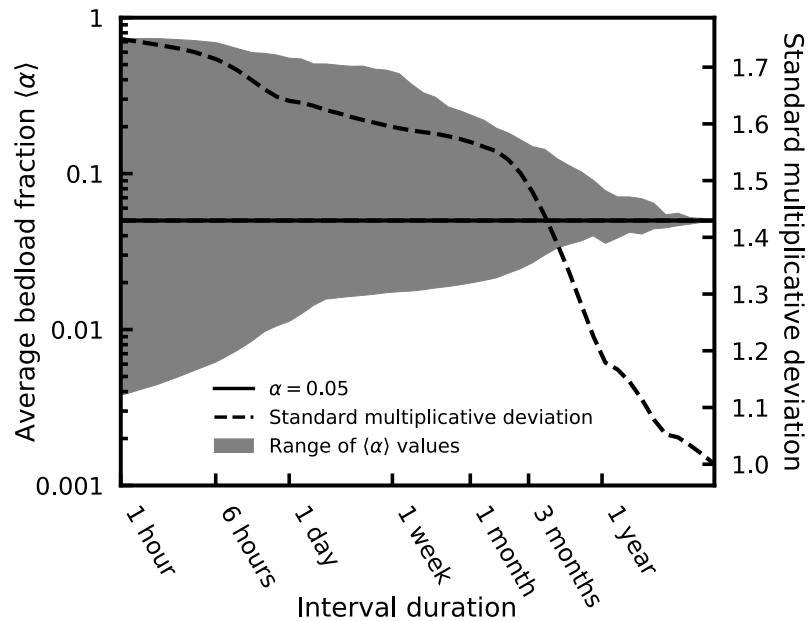


632 **Figure 13.** Plot illustrating the advantages of the proposed model over a constant bedload fraction ap-
 633 proach. Diagonal lines show contours of constant bedload fraction. The predicted (and to a lesser extent,
 634 measured) trend seen here is consistent with the notion that high suspended sand fluxes correspond to elevated
 635 suspension conditions and lower bedload fractions.

642 increases in w_s . Discharge effects are most pronounced before, during, and after controlled
 643 flood experiments (Figure 10), which exemplify both the high and low bedload fraction ex-
 644 tremes. Supply limitation effects are evident during long periods of nearly constant discharge
 645 which tend to be associated with gradual sediment-supply depletion (Figure 11). Gradual de-
 646 pletion causes a concurrent increase in the bedload fraction which is also apparent after the
 647 2014 controlled flood experiment (Figure 10).

648 5.3 Management implications

649 Sediment budgets are used to estimate changes in stored sediment mass over a wide
 650 range of timescales. Short term effects of interest include perturbations related to dam-regulated
 651 water discharge or tributary sand delivery. Serendipitously (in the context of 5% bedload co-
 652 efficients used by *Rubin et al.* [2001]; *Topping et al.* [2010]; *Grams et al.* [2013]), we find
 653 that cumulative bedload discharge was approximately 5% of the cumulative suspended sand
 654 discharge over the nine-year record considered here. However, instantaneous bedload flux
 655 ranges from less than 1% to as much as 75% of suspended sand load depending on water
 656 discharge and the supply-limitation state. As a result, short-term mass-balance fluctuations
 657 caused by experimental changes in discharge regime (i.e. controlled floods), transient ac-
 658 commodation of tributary sand pulses, or prolonged periods of constant discharge are not
 659 adequately represented using a constant bedload fraction or rating curve model for bedload
 660 flux. For example, cumulative bedload during controlled floods is only 2% of cumulative
 661 suspended load during the same intervals, whereas the cumulative bedload is 10% of cu-
 662 mulative suspended load during period when flow is below the mean annual discharge. In
 663 general, the magnitude of deviations in short-term average bedload fraction from a measured
 664 long-term average is a function of averaging timescale (Figure 14)



665 **Figure 14.** Plot illustrating the timescale dependence of the average bedload fraction, $\langle \alpha \rangle$. Average bedload
 666 fraction was computed for every period with the duration indicated on the x axis. The filled gray area spans
 667 the full range of average bedload fractions computed for intervals with the specified duration. The dotted gray
 668 line shows the standard deviation of the average bedload fraction as a function of interval duration. At the
 669 minimum model resolution, bedload fraction may range from 0.004 to 0.74.

670 Over longer timescales, researchers aim to constrain the effects of changes in the water
 671 discharge or sediment delivery regime as dictated by dam protocols, climate, and land use
 672 in the upper Colorado River basin [e.g., Andrews, 1991; Grams *et al.*, 2013; Mueller *et al.*,
 673 2014; Grams *et al.*, 2015; Kasprak *et al.*, 2018; Mueller *et al.*, 2018]. In particular, the dam-
 674 regulated water discharge regime is the primary tool for enacting management decisions
 675 aimed at balancing ecological, social, and economic goals. Nearly three decades of Grand
 676 Canyon research suggests that a return to a more natural, seasonal discharge regime would
 677 induce a desirable geomorphic response. Actionable proposals like the “Fill Mead First”
 678 plan [Schmidt *et al.*, 2016] are designed to balance this and other management objectives
 679 by changing the annual cycle of dam releases, and flux-based sediment budgets are critical
 680 for accurately evaluating the effects and effectiveness of such plans. However, the intended
 681 geomorphic response will necessarily involve changes in channel geometry and bed composi-
 682 tion, affecting sediment flux in a manner that cannot be tracked using traditional rating curve
 683 or bedload fraction approaches. Measurements of q_w , C_s and D_s are indicative of changes in
 684 q_b and such that it is possible to resolve short-term morphodynamic adjustment and evaluate
 685 the effects of future changes in the water discharge and sediment supply regime.

686 5.4 Other applications of modeling approach

687 Bedload has historically been difficult to measure directly. As a result, its role in gov-
 688 erning large-scale river organization poorly understood. Although this paper focuses on es-
 689 timating bedload on the Colorado River, the modeling approach presented herein will en-
 690 able improved estimates of bedload flux in any sand-bedded river. Our model can be applied
 691 retroactively to innumerable historical measurements of suspended sediment concentration
 692 and grain size, providing a new approach for connecting bedload transport to continent- and
 693 basin-scale river dynamics.

694 This work also supports a more general principle that extends beyond the problem of
 695 estimating bedload flux. We have argued that our bedload model provides reliable predic-
 696 tions because it approximates quasi-universal relationships between transport parameters
 697 emerge through the processes governing their interaction and equilibration. In this view,
 698 first order changes in flow and transport conditions including bedload flux, suspended sand
 699 concentration, and suspended sand diameter are driven by three variables: water discharge,
 700 slope, and bed material grain size. This implies that any relevant variable can be estimated
 701 from measurements of three other variables, providing a general formula for constructing
 702 predictive empirical relations in sandy fluvial systems. This strategy may prove useful for re-
 703 constructing hydraulic and transport conditions in scenarios where certain variables are dif-
 704 ficult or impossible to measure, for example in applications involving remotely sensed river
 705 data or measurements of fluvial sedimentary rocks.

706 **6 Conclusions**

707 The modeling approach presented here was developed to estimate reach-averaged bed-
 708 load flux from measurements of water discharge, concentration, and grain size in suspen-
 709 sion. This approach is based on the assumption that most of the variability in sand-bed rivers
 710 can be reduced to three principle modes of variation that are causally attributed to water dis-
 711 charge, slope, and bed grain size. Measurements of concentration and grain size in suspen-
 712 sion provide reliable proxies for the effect of slope and bed material grain size on bedload
 713 flux.

714 Bayesian hierarchical modeling assumes similarity between rivers to ensure efficient
 715 use of limited data. This approach reduces in-sample bias compared with a fully grouped
 716 regression, and it improves parameter estimation precision compared with the ungrouped
 717 regression. However, we anticipate that the general modeling approach presented here may
 718 prove useful in other contexts for which grouped or ungrouped generative data models may
 719 be preferable.

720 We find that predicted bedload flux during the period from 2008 to 2016 averaged over
 721 the full gage record at Diamond Creek is approximately 5% of the measured suspended sed-
 722 iment load. However, instantaneous values deviate significantly from 5% depending on flow
 723 strength and sediment supply conditions. Notably, changes in bedload flux at a constant wa-
 724 ter discharge are indicative of short-term sediment supply enrichment and depletion. Using
 725 the median prediction from the hierarchical model, we find that bedload flux ranges from as
 726 high as 75 % of suspended sand load (during fine-sand depleted, low-discharge periods) to
 727 less than 1% (during fine-sand enriched floods). The decade-average bedload fraction is ex-
 728 pected to deviate systematically from 5% in the future if bed composition and channel geom-
 729 etry evolve due to changes in tributary sand supply or the dam-regulated discharge regime.
 730 In order to ensure accurate quantification of fluctuations in sediment storage over a range of
 731 timescales, it is critical to account for deviations in the ratio of bedload to suspended load
 732 driven both by individual events (for example, high flow experiments or tributary floods) and
 733 long-term evolution of channel geometry and bed composition.

734 **A: Estimating bedload flux from repeat bathymetric surveys of dune migration**

735 Bedload flux estimates at our site were computed from point clouds of bed topography
 736 obtained at approximately six-minute intervals. This was accomplished using the following
 737 procedure:

- 738 1. Flow direction is determined by inspection and point clouds are transformed to stream-
 739 wise and cross-stream coordinates.

- 740 2. An upstream and downstream extent is chosen to bracket a region of the bed used for
 741 computation of flux. The region used here is largest region where the margins of the
 742 bedform field are parallel and bedform geometry appears to be uniform in all surveys.
 743 3. Point clouds are divided by cross-stream coordinate into streamwise oriented transects
 744 spaced at 25 cm.
 745 4. Ungridded points that fall within each 25 cm-wide transect are gridded at a 10 cm
 746 streamwise resolution using a locally-weighted nonparametric filter.
 747 5. Transects are detrended using a high-pass Fourier filter. The filter wavelength used
 748 here is three times the largest dune length determined by inspection.
 749 6. Characteristic bedform height is estimated as $2\sqrt{2} * \sigma_\eta$ where σ_η is the root mean
 750 squared detrended bed elevation [McElroy, 2009]
 751 7. A matrix of dune displacements (determined from the maximum of the cross-correlation
 752 function) is computed for each transect using every pair of surveys. Valid displace-
 753 ments are retained to calculate migration rate according to the following criteria: (a)
 754 temporal separation is not greater than one hour, (b) displacement is not greater than
 755 20 percent of the bedform length, determined from the spectral centroid of the de-
 756 trended bed profile [Van der Mark & Blom, 2007], (c) the maximum of the cross cor-
 757 relation function is not less than 0.8, and (d) the implied migration rate (displacement
 758 divided by temporal separation) is not greater than 3 meters per hour and not less than
 759 0.3 meters per hour. These criteria optimize temporal resolution and stability of the
 760 bedload flux calculation, and reliably discriminate transects with active dune evolu-
 761 tion from plane-bed topography.
 762 8. Bedform migration rate is computed for each transect using ordinary least-squares
 763 regression forced through the origin with all valid displacements.
 764 9. Volumetric bedload flux per unit width is computed for each streamwise transect us-
 765 ing the bedform bedload equation [Simons *et al.*, 1965].
 766 10. Total bedload mass flux was computed for each transect by multiplying unit bed-
 767 load flux by the transect width (25 cm) and the density of quartz (2650 kg/m^3), then
 768 summed.

769 We find that the bedform migration rate regression using displacements forward and back-
 770 ward in time is necessary to ensure stable results. However, this means that bedload flux es-
 771 timates are derived from overlapping data. Down sampling is thus necessary to ensure that
 772 each reported value of bedload flux is computationally independent: we consider a maximum
 773 temporal resolution of one hour. Results are plotted in Figure 4.

774 B: Bayesian regression

775 Here, we provide additional details on the statistical techniques employed in this pa-
 776 per. In order to make this explanation more clear, we adopt notation that is common in sta-
 777 tistical literature [e.g. Gelman *et al.*, 1995; Christensen *et al.*, 2011]. We consider the prob-
 778 lem of predicting a continuous response variable y from a vector of predictor variables $\bar{\mathbf{x}} =$
 779 $[1, x_1, x_2, x_3]$. The relationship between predictor variables and response variables is studied
 780 using a probabilistic model with parameters θ for the data generating process.

781 Physical variables of interest are log-transformed and normalized to obtain linear pre-
 782 dictor and response variables such that $y = \log(q_b/q_{b0})$, $x_1 = \log(Q/Q_0)$, $x_2 = \log(C_s/C_{s0})$
 783 and $x_3 = \log(D_s/D_{s0})$ and The subscript 0 denotes the geometric mean of all observations,
 784 which is equivalent to subtracting the arithmetic mean of log-transformed variables and re-
 785 sults in centered response and predictor variables. This is a convention that facilitates inter-
 786 pretation of the intercept term β_0 . The subscript i denotes a specific observation such that y_i
 787 and $\bar{\mathbf{x}}_i$ are the i^{th} of n observations of response and predictor variables, respectively. A cap-
 788 ital X is short hand for all observations of model variables, i.e. $X = (\bar{\mathbf{x}}_0, \dots, \bar{\mathbf{x}}_n, y_0, \dots, y_n)$.
 789 Finally, we use $\tilde{\mathbf{x}}_i$ to denote a vector of observations of predictor variables for which we in-
 790 tend to predict an unobserved value of the response variable, \tilde{y}_i .

791

B.1 Grouped model

792

793

794

795

796

797

798

799

The grouped model ignores potential correlations that may exist on a site specific basis. All data is pooled into a single normal linear regression analysis. Regression coefficients and errors are assumed to be equivalent at all sites. Here, $\boldsymbol{\beta} = [\beta_0, \beta_1, \beta_2, \beta_3]$ is a 1×4 vector of regression coefficients. The i^{th} observation of the response variable y_i is modeled as a linear function of predictor variables plus a normally-distributed independent error term (e.g. equation 8). This is equivalent to specifying that the y_i follows a normal distribution with mean $\boldsymbol{\beta}\bar{\mathbf{x}}_i$ and standard deviation σ . Formally, the probability of observing y_i given $\bar{\mathbf{x}}_i$, $\boldsymbol{\beta}$, and σ is given by:

$$p(y_i|x_i, \boldsymbol{\beta}, \sigma) = \frac{1}{\sqrt{2\pi\sigma^2}} \exp\left[-\frac{(y_i - \boldsymbol{\beta}x_i)^2}{2\sigma^2}\right] \quad (\text{B.1})$$

800

801

and the likelihood of model parameters $\theta = (\boldsymbol{\beta}, \sigma)$ conditional on all observational data $X = (x_0, \dots, x_n, y_0 \dots y_n)$ is simply the product of the probabilities of each individual observation:

$$L(\theta|X) = \prod_{i=1}^n p(y_i|x_i, \boldsymbol{\beta}, \sigma). \quad (\text{B.2})$$

802

803

For the grouped model, we employ the following independent priors for model parameters:

$$\beta_0 \sim \mathcal{N}(0, 100) \quad (\text{B.3})$$

$$\beta_1 \sim \mathcal{N}(0, 100) \quad (\text{B.4})$$

$$\beta_2 \sim \mathcal{N}(0, 100) \quad (\text{B.5})$$

$$\beta_3 \sim \mathcal{N}(0, 100) \quad (\text{B.6})$$

$$\sigma \sim \Gamma^{-1}(0.001, 0.001). \quad (\text{B.7})$$

804

805

806

807

808

Here, $\mathcal{N}(\mu, \sigma)$ denotes a normal distribution with mean μ and standard deviation σ , and $\Gamma^{-1}(\alpha_1, \alpha_2)$ denotes the inverse gamma distribution with shape parameter α_1 and scale parameter α_2 . Since the marginal priors are independent, $p(\boldsymbol{\beta}, \sigma) = p(\beta_0)p(\beta_1)p(\beta_2)p(\beta_3)p(\sigma)$. These priors approximate Jeffrey's prior for normal linear regression which is a uniform distribution on $(\boldsymbol{\beta}, \log(\sigma))$ [Gelman *et al.*, 1995; Christensen *et al.*, 2011].

809

810

The posterior probability distribution of model parameters θ given data X is proportional to the product of the likelihood function and the prior:

$$P(\theta|X) = \frac{L(\theta|X)P(\theta)}{\int L(\theta|X)P(\theta)d\theta}, \quad (\text{B.8})$$

811

812

where the constant of proportionality $[\int L(\theta|X)P(\theta)d\theta]^{-1}$ ensures that the posterior integrates to 1.

813

B.2 Ungrouped model

814

815

816

817

818

819

The ungrouped model involves fitting separate regression models for each site. Henceforth, the subscript $j = 1, \dots, m$ denotes the j^{th} of $m = 8$ sites. $\boldsymbol{\beta}_j = [\beta_{0j}, \beta_{1j}, \beta_{2j}, \beta_{3j}]$ is thus the vector of regression coefficients corresponding to site j , and σ_j is the standard deviation of the error term at site j . The full data model thus contains $4 \times m$ regression coefficients and m error terms, totaling 40 parameters compared with the 5 parameters used in the ungrouped model.

820

821

Each site has a different number of observations, n_j . The probability of observing i^{th} of n_j observations of the response variable at site j , $y_{i,j}$ given $x_{i,j}$, $\boldsymbol{\beta}_j$, and σ_j is given by

$$p(y_{i,j}|x_{i,j}, \boldsymbol{\beta}_j, \sigma_j) = \frac{1}{\sqrt{2\pi\sigma_j^2}} \exp\left[-\frac{(y_{i,j} - \boldsymbol{\beta}_j x_{i,j})^2}{2\sigma_j^2}\right] \quad (\text{B.9})$$

822 and the likelihood function of model parameters $\theta = (\beta_0, \dots, \beta_m, \sigma_0, \dots, \sigma_m)$ conditional on
 823 all observational data X is given by the product of the probabilities of all observations:

$$L(\theta|X) = \prod_{j=1}^m \prod_{i=1}^{n_j} (y_{i,j}|x_{i,j}, \beta_j, \sigma_j) \quad (\text{B.10})$$

824 Separate independent priors are used for each site, i.e:

$$\beta_{0j} \sim \mathcal{N}(0, 100) \quad (\text{B.11})$$

$$\beta_{1j} \sim \mathcal{N}(0, 100) \quad (\text{B.12})$$

$$\beta_{2j} \sim \mathcal{N}(0, 100) \quad (\text{B.13})$$

$$\beta_{3j} \sim \mathcal{N}(0, 100) \quad (\text{B.14})$$

$$\sigma_j \sim \Gamma^{-1}(0.001, 0.001). \quad (\text{B.15})$$

825 B.3 Hierarchical Model

826 Like the ungrouped model, the hierarchical model involves fitting separate regression
 827 coefficients for each site. However, unlike the ungrouped model, these regression coefficients
 828 are assumed to come from a common distribution that encompasses the range of parameters
 829 that exist in sand bed rivers. Additionally, there a single error term σ is applied at all sites.
 830 Instead of using separate, diffuse priors with fixed parameters for the regression coefficients
 831 at each site, informative, dynamic priors are used, i.e.:

$$\beta_{0j} \sim \mathcal{N}(\mu_{\beta_0}, \varsigma_{\beta_0}) \quad (\text{B.16})$$

$$\beta_{1j} \sim \mathcal{N}(\mu_{\beta_1}, \varsigma_{\beta_1}) \quad (\text{B.17})$$

$$\beta_{2j} \sim \mathcal{N}(\mu_{\beta_2}, \varsigma_{\beta_2}) \quad (\text{B.18})$$

$$\beta_{3j} \sim \mathcal{N}(\mu_{\beta_3}, \varsigma_{\beta_3}) \quad (\text{B.19})$$

$$\sigma \sim \Gamma^{-1}(0.001, 0.001). \quad (\text{B.20})$$

832 Here, $\psi = (\mu_{\beta_0}, \mu_{\beta_1}, \mu_{\beta_2}, \mu_{\beta_3}, \varsigma_{\beta_0}, \varsigma_{\beta_1}, \varsigma_{\beta_2}, \varsigma_{\beta_3})$ are known as hyperparameters; μ terms are
 833 the mean of the prior on the regression coefficients and represent the central tendency of sites
 834 in our data set (as a proxy for sand bed rivers), while ς terms are the standard deviation of
 835 the priors and represent the variability present across sites in our dataset. Because the priors
 836 depend on dynamic hyperparameters, the posterior probability takes a slightly different form:

$$p(\theta|X) = \frac{L(\theta|X)P(\theta|\psi)P(\psi)}{\int [L(\theta|X)P(\theta|\psi)P(\psi)]d\theta d\psi}, \quad (\text{B.21})$$

837 where $P(\theta|\psi)$ is the prior probability distribution for model parameters θ given hyperparamete-
 838 rs ψ , and $P(\psi)$ is the prior probability distribution for ψ , or the hyperprior. Reported results
 839 were obtained using the following diffuse, independent hyperpriors:

$$\mu_k \sim \mathcal{N}(0, 100) \quad (\text{B.22})$$

$$\varsigma_k \sim \Gamma^{-1}(0.001, 0.001) \quad (\text{B.23})$$

840 for $k = 0, 1, 2, 3$. The grouped and ungrouped models can be framed as special cases of the
 841 hierarchical model with informative hyperpriors. Specifically, the grouped model is a case
 842 where $\varsigma_k \sim \delta(0)$, where δ is the dirac delta function. This leads to $\beta_k = \mu_k$ for all sites.
 843 The ungrouped model is a case where $\mu_k \sim \delta(0)$ and $\varsigma_k \sim \delta(100)$ such that the hyperpriors
 844 exert minimal influence on β_k .

845 B.4 MCMC sampling

846 Posterior distributions for model parameters were constructed using the No-U-Turn
 847 sampling (NUTS) algorithm [Hoffman & Gelman, 2014], as implemented in the open source

848 Python package, PyMC3 [Salvatier et al., 2016]. The sampler was initiated using the auto-
 849 matic differentiation variational inference algorithm [Kucukelbir et al., 2016]. Three chains
 850 were used, and 1000 burn-in steps were more than sufficient to achieve convergence. The
 851 posterior distribution of model parameters was approximated using 5000 steps without thin-
 852 ning.

853 B.5 Prediction

854 Once the posterior probability distribution of model parameters is known, unobserved
 855 values of the response variable \tilde{y}_i can be estimated using Bayesian posterior predictive dis-
 856 tributions. The posterior predictive density $P(\tilde{y}_i|\tilde{x}_i, X)$ is found by integrating the sampling
 857 distribution of \tilde{y}_i given a specific set of parameters, $p(\tilde{y}_i|\tilde{x}_i, \theta)$, against the posterior distribu-
 858 tion of model parameters, $P(\theta|X)$:

$$P(\tilde{y}_i|\tilde{x}_i, X) = \int P(\tilde{y}_i|\tilde{x}_i, \theta)P(\theta|X)d\theta. \quad (\text{B.24})$$

859 This distribution is straightforward to compute numerically using MCMC techniques.
 860 In addition to predicting single unobserved values of q_b , it is possible to obtain a simulated
 861 predictive distribution for any conceivable quantity that can be expressed as a function of
 862 model parameters (for example, time-integrated bedload flux).

863 B.6 Deviance Information Criterion

864 The Deviance Information Criterion (DIC) is a measure of relative predictive power
 865 that reflects the trade-off between goodness of fit and parameter estimation precision [Spiegel-
 866 halter et al., 2002; Gelman et al., 2014]. It is used here instead of other more well-known
 867 model selection criteria like the Akaike information criterion (AIC) or the Bayesian infor-
 868 mation criterion (BIC) because unlike AIC, it is suitable for comparing the hierarchical and
 869 non-hierarchical models considered here, and unlike BIC, its intended use is for comparing
 870 expected out-of-sample predictive accuracy under the assumption that the data model is cor-
 871 rect.

872 DIC uses the log-likelihood $\log L(\theta|X)$ of different models to compare expected out
 873 of sample predictive accuracy. Models that achieve higher values of the likelihood function
 874 provide better in-sample fit. The log-likelihood of the posterior mean parameter estimate
 875 $\log L(\bar{\theta}|X)$ is used here to quantify model fit. For clarity, $\bar{\theta} = E(\theta|X)$ is the posterior mean
 876 parameter estimate.

877 More complex models may lead to higher log-posterior densities and better in-sample
 878 fit at the cost of parameter estimation precision. In other words, a much wider range of model
 879 parameters provide a good fit to the data such that it is difficult to select optimal values. For
 880 models that are too complex, predictive uncertainty is primarily related to uncertainty in
 881 model parameters rather than being directly quantified by the noise term (σ in the models
 882 presented here). It is thus necessary to introduce a correction factor that accounts for param-
 883 eter estimation uncertainty. Here, the effective number of parameters $p_{DIC} = 2\text{var}_{post}(\log L(\theta|X))$
 884 is framed in terms of the posterior variance in the log-likelihood, and can be computed by
 885 taking the variance of MCMC sampled log-likelihoods.

886 The expected log predictive density is given by $elpd = \log L(\bar{\theta}|X) - p_{DIC}$. Assuming
 887 predictive error is normally distributed, the expected log predictive density is proportional to
 888 the mean squared error. DIC is related to the expected log posterior density by a factor of
 889 -2 due to convention:

$$DIC = -2 \log L(\bar{\theta}|X) + 2p_{DIC} \quad (\text{B.25})$$

890 For additional details on the derivation and interpretation of DIC, see *Spiegelhalter et*
 891 *al.* [2002]; Gelman et al. [2014].

892 Acknowledgments

893 We thank Bob Tusso, Dan Hamill, and Erich Mueller their help in the field. U.S. Geological
 894 Survey studies in Grand Canyon are supported by the Grand Canyon Dam Adaptive Manage-
 895 ment Program administered by the U.S. Department of the Interior Bureau of Reclamation.
 896 Additional support was provided by the University of Wyoming School of Energy Resources.
 897 Data and software supporting the analysis and conclusions presented here are available on-
 898 line through the SEAD data repository and github [Leary, 2018; Ashley, 2019a,b]. Any use
 899 of trade, product, or firm names is for descriptive purposes only and does not imply endorse-
 900 ment by the U.S. Government.

901 References

- 902 Ashley, T. (2019) qDune version 1.0 [Computer Software]
 903 <https://doi.org/10.5281/zenodo.3515483>
- 904 Ashley, T. (2019) qbStats version 1.0 [Computer Software]
 905 <https://doi.org/10.5281/zenodo.3515485>
- 906 Andrews, E. D. (1991). Sediment transport in the Colorado River basin. In *Colorado River*
 907 *Ecology and Dam Management: Proceedings of a Symposium* (pp. 54–74). Washington,
 908 DC: National Academies Press.
- 909 Brownlie, W. R. (1983). Flow depth in sand-bed channels. *Journal of Hydraulic Engineer-*
 910 *ing*, 109(7), 959–990.
- 911 Buscombe, D., Rubin, D. M., & Warrick, J. A. (2010). A universal approximation of grain
 912 size from images of noncohesive sediment. *Journal of Geophysical Research: Earth Sur-*
 913 *face*, 115, F02015. <https://doi.org/10.1029/2009JF001477>
- 914 Buscombe, D., Grams, P. E., & Kaplinski, M. A. (2014a). Characterizing riverbed sediment
 915 using high-frequency acoustics: 1. Spectral properties of scattering. *Journal of Geophys-*
 916 *ical Research: Earth Surface*, 119, 2674–2691. <https://doi.org/10.1002/2014JF003189>
- 917 Buscombe, D., Grams, P. E., & Kaplinski, M. A. (2014b). Characterizing riverbed sediment
 918 using high-frequency acoustics: 2. Scattering signatures of Colorado Riverbed sediment in
 919 Marble and Grand Canyons. *Journal of Geophysical Research: Earth Surface*, 119, 2692–
 920 2710. <https://doi.org/10.1002/2014JF003191>
- 921 Christensen, R., Johnson, W., Branscum, A., & Hanson, T. E. (2011). *Bayesian ideas and*
 922 *data analysis: An introduction for scientists and statisticians*. Boca Raton, FL: Chapman
 923 Hall.
- 924 Dean, D. J., Topping, D. J., Schmidt, J. C., Griffiths, R. E., & Sabol, T. A., (2016). Sedi-
 925 ment supply versus local hydraulic controls on sediment transport and storage in a river
 926 with large sediment loads, *Journal of Geophysical Research: Earth Surface* 121, 82–110,
 927 <https://doi.org/10.1002/2015JF003436>.
- 928 Dolan, R., Howard, A., & Gallenson, A. (1974), Man's impact on the Colorado River in the
 929 Grand Canyon: The Grand Canyon is being affected both by the vastly changed Colorado
 930 River and by the increased presence of man. *American Scientist*, 62(4), 392–401.
- 931 Einstein, H. A. (1950). The bed load function in open channel flows. *U.S. Dept. of Agricul-*
 932 *ture Technical Bulletin No. 1026*.
- 933 Einstein, H. A., & Chien, N. (1953). Can the rate of wash load be predicted from the
 934 bedload function?. *Eos, Transactions American Geophysical Union*, 34(6), 876-882.
- 935 Ellison, C. A., Groten, J. T., Lorenz, D. L., & Koller, K. S. (2016). Application of dimension-
 936 less sediment rating curves to predict suspended-sediment concentrations, bedload, and
 937 annual sediment loads for rivers in Minnesota. *USGS Scientific Investigations Report No.*
 938 *2016-5146*.

- 939 Emmett, W. W., & Wolman, M. G. (2001). Effective discharge and gravel-bed rivers. *Earth*
 940 *Surface Processes and Landforms*, 26(13), 1369–1380. <https://doi.org/10.1002/esp.303>
- 941 Engel, P., and Lau, Y. L. (1980), Computation of bed load using bathymetric data. *Journal*
 942 *of the Hydraulics Division of the American Society of Civil Engineers*, 106(HY3), 369–380.
 943 380.
- 944 Engelund, F., & Hansen, E. (1967). A monograph on sediment transport in alluvial streams.
 945 *Technisk Forlag, Copenhagen, Denmark*.
- 946 Gaeuman, D., & Jacobson, R. B. (2007). Field assessment of alternative bed-load transport
 947 estimators. *Journal of Hydraulic Engineering*, 133(12), 1319–1328.
- 948 Garcia, M. (2008), Sediment transport and morphodynamics. In *Sedimentation Engineering:*
 949 *Process, Management, Modeling and Practice* (pp. 21–163). Reston, VA: ASCE.
- 950 Garcia, M., & Parker, G. (1991). Entrainment of bed sediment into suspension. *Journal of*
 951 *Hydraulic Engineering*, 117(4), 414–435.
- 952 Gelman, A., Carlin, J. B., Stern, H. S., Dunson, D. B., Vehtari, A., & Rubin, D. B. (1995).
 953 *Bayesian data analysis*. Chapman and Hall/CRC.
- 954 Gelman, A., Hwang, J., & Vehtari, A. (2014). Understanding predictive informa-
 955 tion criteria for Bayesian models. *Statistics and computing*, 24(6), 997–1016.
 956 <https://doi.org/10.1007/s11222-013-9416-2>
- 957 Gibbings, J. C. (2011). The Pi-Theorem. In *Dimensional Analysis* (pp. 55–82). Springer, Lon-
 958 don.
- 959 Grams, P. E., Topping, D. J., Schmidt, J. C., Hazel, J. E., & Kaplinski, M. (2013). Linking
 960 morphodynamic response with sediment mass balance on the Colorado River in Marble
 961 Canyon: Issues of scale, geomorphic setting, and sampling design. *Journal of Geophysical*
 962 *Research: Earth Surface*, 18(2), 361–381. <https://doi.org/doi:10.1002/jgrf.20050>
- 963 Grams, P. E., Schmidt, J. C., Wright, S. A., Topping, D. J., Melis, T. S., & Rubin, D. M.
 964 (2015). Building sandbars in the Grand Canyon. *EOS: Transactions of the American Geo-*
 965 *physical Union*, 96, 1–11. <https://doi.org/doi:10.1002/jgrf.20050>
- 966 Grams, P. E., Buscombe, D., Topping, D. J., Kaplinski, M., & Hazel, J. E. (2018). How many
 967 measurements are required to construct an accurate sand budget in a large river? Insights
 968 from analyses of signal and noise. *Earth Surface Processes and Landforms*, 44, 160–178.
 969 <https://doi.org/10.1002/esp.4489>
- 970 Gray, J. R., Gartner, J. W., Barton, J. S., Gaskin, J., Pittman, S. A., & Rennie, C. D. (2010).
 971 Surrogate technologies for monitoring bed-load transport in rivers. *Sedimentology of*
 972 *Aqueous Systems*, 2, 45–79.
- 973 Gray, J. R., & Gartner, J. W. (2009). Technological advances in suspended-sediment surro-
 974 gate monitoring. *Water resources research*, 45(4). <https://doi.org/10.1029/2008WR007063>
- 975 Hastie, T., Tibshirani, R., & Friedman, J. H. (2009). Model assessment and selection. In *The*
 976 *Elements of Statistical Learning: Data Mining, Inference, and Prediction*, (pp. 219–260).
 977 New York, NY: Springer.
- 978 Hoffman, M. D., & Gelman, A. (2014). The No-U-turn sampler: adaptively setting path
 979 lengths in Hamiltonian Monte Carlo. *Journal of Machine Learning Research*, 15(1),
 980 1593–1623. <https://arxiv.org/pdf/1111.4246>
- 981 Holmes, R. R. (2010). Measurement of bedload transport in sand-bed rivers: A look at two
 982 indirect sampling methods. *US Geological Survey Scientific Investigations Report*, 5091,
 983 236–252.
- 984 Ingram, H., Tarlock, A. D., & Oggins, C. R. (1991), The law and politics of the operation of
 985 Glen Canyon Dam. In *Colorado River Ecology and Dam Management: Proceedings of a*
 986 *Symposium* (pp. 10–27), Washington, DC: National Academies Press.
- 987 Minckley, W. L. (1991). Native fishes of the Grand Canyon region: an obituary. In *Colorado*
 988 *River Ecology and Dam Management: Proceedings of a Symposium* (pp. 124–177), Wash-
 989 ington, DC: National Academies Press.
- 990 Kaplinski, M., Hazel, J. E., Parnell, R., Breedlove, M., Kohl, K., & Gonzales, M. (2009).
 991 Monitoring fine-sediment volume in the Colorado River ecosystem, Arizona; Bathymetric
 992 survey techniques *U.S. Geological Survey Open-File Report 2009-1207*.

- 993 Kaplinski, M., Hazel Jr, J. E., Grams, P. E., & Davis, P. A. (2014). Monitoring fine-
 994 sediment volume in the Colorado River ecosystem, Arizona: Construction and analy-
 995 sis of digital elevation models *U.S. Geological Survey Open-File Report 2014-1052*.
 996 <https://dx.doi.org/10.3133/ofr20141052>
- 997 Kasprak, A., Sankey, J. B., Buscombe, D., Caster, J., East, A. E., & Grams, P. E. (2018).
 998 Quantifying and forecasting changes in the areal extent of river valley sediment in re-
 999 sponse to altered hydrology and land cover *Progress in Physical Geography: Earth and*
 1000 *Environment*, 42(6), 739–764. <https://doi.org/10.1177/0309133318795846>
- 1001 Kucukelbir, A., Tran, D., Ranganath, R., Gelman, A., & Blei, D. M. (2017). Automatic dif-
 1002 ferentiation variational inference. *The Journal of Machine Learning Research*, 18(1), 430–
 1003 474. <https://arxiv.org/pdf/1603.00788.pdf>
- 1004 Leary, K. (2018). Diamond Creek Repeat Multibeam Data, *SEAD Internal Repository*,
 1005 <http://doi.org/10.5967/M02J6904>
- 1006 Leopold, L. B., & Maddock, T. (1953). The hydraulic geometry of stream channels and some
 1007 physiographic implications *U.S. Geological Survey Professional Paper 252*.
- 1008 McElroy, B. J. (2009). Expressions and implications of sediment transport variability in
 1009 sandy rivers (PhD Dissertation). <http://hdl.handle.net/2152/15117>
- 1010 McLean, S. R. (1992). On the calculation of suspended load for noncohesive
 1011 sediments. *Journal of Geophysical Research: Oceans*, 97(C4), 5759–5770.
 1012 <https://doi.org/10.1029/91JC02933>
- 1013 Meyer-Peter, E., & Müller, R. (1948). Formulas for bed-load transport. In *IAHSR 2nd meet-*
 1014 *ing*, Stockholm: IAHR.
- 1015 Mohrig, D., & Smith, J. D. (1996). Predicting the migration rates of subaqueous dunes. *Wa-*
 1016 *ter Resources Research*, 32(10), 3207–3217.
- 1017 Molinas, A., and Wu, B. (2000). Comparison of fractional bed-material load computation
 1018 methods in sand-bed channels. *Earth Surface Processes and Landforms*, 25, 1045–1068.
- 1019 Mueller, E. R., Grams, P. E., Schmidt, J. C., Hazel, J. E., Alexander, J. S., & Kaplin-
 1020 ski, M. (2014). The influence of controlled floods on fine sediment storage in de-
 1021 bris fan-affected canyons of the Colorado River basin. *Geomorphology*, 226, 65–75.
 1022 <https://doi.org/10.1016/j.geomorph.2014.07.029>
- 1023 Mueller, E. R., Grams, P. E., Hazel, J. E., & Schmidt, J. C. (2018). Variability
 1024 in eddy sandbar dynamics during two decades of controlled flooding of the
 1025 Colorado River in the Grand Canyon. *Sedimentary Geology*, 363, 181–199.
 1026 <https://doi.org/10.1016/j.sedgeo.2017.11.007>
- 1027 Paola, C., & Voller, V. R. (2005). A generalized Exner equation for sediment
 1028 mass balance. *Journal of Geophysical Research: Earth Surface*, 110(F4).
 1029 <https://doi.org/10.1029/2004JF000274>
- 1030 Pitlick, J. (1988). Variability of bed load measurement. *Water Resources Research*, 24(1),
 1031 173–177. <https://doi.org/10.1029/WR024i001p00173>
- 1032 Rantz, S. E., et al. (1982). Measurement and computation of streamflow, *U.S. Geological*
 1033 *Survey Water Supply Paper 2175*.
- 1034 Rubin, D. M., Tate, G. B., Topping, D. J., & Anima, R. A. (2001). Use of rotating side-scan
 1035 sonar to measure bedload. *Proceedings of the Seventh Federal Interagency Sedimentation*
 1036 *Conference* (pp. 139–144). Reno, NV: U.S. Geological Survey
- 1037 Rubin, D. M., & Topping, D. J. (2001). Quantifying the relative importance of flow
 1038 regulation and grain size regulation of suspended sediment transport α and tracking
 1039 changes in grain size of bed sediment β . *Water Resources Research*, 37(1), 133–146.
 1040 <https://doi.org/10.1029/2000WR900250>
- 1041 Rubin, D. M., Topping, D. J., Schmidt, J. C., Hazel, J., Kaplinski, M., & Melis, T. S. (2002).
 1042 Recent sediment studies refute Glen Canyon Dam hypothesis. *Eos, Transactions American*
 1043 *Geophysical Union*, 83(25), 273–278. <https://doi.org/10.1029/2002EO000191>
- 1044 Salvatier, J., Wiecki, T. V., & Fonnesbeck, C. (2016). Probabilistic programming in Python
 1045 using PyMC3. *PeerJ Computer Science* 2:e55. <https://doi.org/10.7717/peerj-cs.55>

- 1046 Schmelter, M. L., Hooten, M. B., & Stevens, D. K. (2011). Bayesian sediment transport
1047 model for unisize bed load. *Water Resources Research*, 47(11).
- 1048 Schmelter, M. L., & Stevens, D. K. (2012). Traditional and Bayesian statistical models in
1049 fluvial sediment transport. *Journal of Hydraulic Engineering*, 139(3), 336-340.
- 1050 Schmelter, M. L., Erwin, S. O., & Wilcock, P. R. (2012). Accounting for uncertainty in cu-
1051 mulative sediment transport using Bayesian statistics. *Geomorphology*, 175, 1-13.
- 1052 Schmelter, M., Wilcock, P., Hooten, M., & Stevens, D. (2015). Multi-fraction Bayesian sedi-
1053 ment transport model. *Journal of Marine Science and Engineering*, 3(3), 1066-1092.
- 1054 Schmidt, J. C., and J. B. Graf (1990). Aggradation and degradation of alluvial sand deposits,
1055 1965 to 1986, Colorado River, Grand Canyon National Park, Arizona, *US Geological Sur-
1056 vey Professional Paper 1493*.
- 1057 Schmidt, J. C., Kraft, M., Tuzlak, D., and Walker, A. (2016). Fill mead first: A technical
1058 assessment. *White Paper No. 1*, Utah State University Quinney College of Natural Re-
1059 sources, Center for Colorado River Studies.
- 1060 Simons, D. B., Richardson, E. V., & Nordin, C. F. (1965). Bedload Equation for Ripples and
1061 Dunes. *U.S. Geological Survey Professional Paper 462-H*.
- 1062 Spiegelhalter, D. J., Best, N. G., Carlin, B. P., & Van Der Linde, A. (2002). Bayesian mea-
1063 sures of model complexity and fit. *Journal of the Royal Statistical Society: Series B (Sta-
1064 tistical Methodology)*, 64(4), 583–639. <https://doi.org/10.1111/1467-9868.00353>
- 1065 Toffaleti, F. B. (1968) A procedure for computation of the total river sand discharge and de-
1066 tailed distribution, bed to surface. *Corps of Engineers Committee on Channel Stabiliza-
1067 tion Technical report number 5*.
- 1068 Topping, D. J., Rubin, D. M., & Vierra, L. E. (2000). Colorado River sediment transport:
1069 1. Natural sediment supply limitation and the influence of Glen Canyon Dam. *Water Re-
1070 sources Research*, 36(2), 515–542. <https://doi.org/10.1029/1999WR900285>
- 1071 Topping, D. J., Rubin, D. M., Nelson, J. M., Kinzel, P. J., & Corson, I. C. (2000).
1072 Colorado River sediment transport: 2. systematic bed-elevation and grain-size
1073 effects of sand supply limitation. *Water Resources Research*, 36(2), 543–570.
1074 <https://doi.org/10.1029/1999WR900286>
- 1075 Topping, D. J., Rubin, D. M., Grams, P. E., Griffiths, R. E., Sabol, T. A., Voichick, N. et al.
1076 (2010). Sediment transport during three controlled-flood experiments on the Colorado
1077 River downstream from Glen Canyon Dam, with implications for eddy-sandbar deposition
1078 in Grand Canyon National Park, *U.S. Geological Survey Open-File Report 2010–1128*.
- 1079 Topping, D. J., & Wright, S. A. (2016). Long-term continuous acoustical suspended-
1080 sediment measurements in rivers – Theory, application, bias, and error. *USGS Professional
1081 Paper 1823*. <https://doi.org/10.3133/pp1823>
- 1082 Topping, D. J., Melis, T. S., Rubin, D. M., & Wright, S. A. (2004). High-resolution monitor-
1083 ing of suspended-sediment concentration and grain size in the Colorado River in Grand
1084 Canyon using a laser-acoustic system. In *Proceedings of the Ninth International Sympo-
1085 sium on River Sedimentation* (pp. 2507–2514). Yichang, China.
- 1086 Topping, D. J., Wright, S. A., Melis, T. S., & Rubin, D. M. (2007). High-resolution measure-
1087 ments of suspended-sediment concentration and grain size in the Colorado River in Grand
1088 Canyon using a multi-frequency acoustic system. In *Proceedings of the Tenth International
1089 Symposium on River Sedimentation* (Vol. 3). Moscow, Russia.
- 1090 Turowski, J. M., Rickenmann, D., & Dadson, S. J. (2010). The partitioning of the total sedi-
1091 ment load of a river into suspended load and bedload: a review of empirical data. *Sedi-
1092 mentology*, 57(4), 1126–1146.
- 1093 van den Berg, J. H. (1987). Bedform migration and bed-load transport in some rivers and
1094 tidal environments. *Sedimentology*, 34(4), 681–698.
- 1095 van der Mark, C. F., & Blom, A. (2007). A new and widely applicable bedform tracking tool.
1096 *Technical Report*, University of Twente, Faculty of Engineering Technology, Department
1097 of Water Engineering and Management.
- 1098 van Rijn, L. C. (1984). Sediment transport, part II: Suspended load transport. *Journal of
1099 Hydraulic Engineering*, 110(11), 1613–1641. [–34–](https://doi.org/10.1061/(ASCE)0733-</p>
</div>
<div data-bbox=)

- 1100 9429(1984)110:11(1613)
- 1101 Wong, M., & Parker, G. (2006). Reanalysis and correction of bed-load relation of Meyer-
- 1102 Peter and Müller using their own database. *Journal of Hydraulic Engineering*, *132*(11),
- 1103 1159–1168. [https://doi.org/10.1061/\(ASCE\)0733-9429\(2006\)132:11\(1159\)](https://doi.org/10.1061/(ASCE)0733-9429(2006)132:11(1159))
- 1104 Wright, S. A., & Kaplinski, M. (2011). Flow structures and sandbar dynamics in a canyon
- 1105 river during a controlled flood, Colorado River, Arizona. *Journal of Geophysical Re-*
- 1106 *search: Earth Surface*, *116*(F1). <https://doi.org/10.1029/2009JF001442>
- 1107 Wright, S., & Parker, G. (2004). Flow resistance and suspended load in sand-bed rivers:
- 1108 simplified stratification model. *Journal of Hydraulic Engineering*, *130*(8), 796–805.
- 1109 [https://doi.org/10.1061/\(ASCE\)0733-9429\(2004\)130:8\(796\)](https://doi.org/10.1061/(ASCE)0733-9429(2004)130:8(796))
- 1110 Wright, S. A., Topping, D. J., Rubin, D. M., & Melis, T. S. (2010). An approach for mod-
- 1111 eling sediment budgets in supply-limited rivers. *Water Resources Research*, *46*(10).
- 1112 <https://doi.org/10.1029/2009WR008600>